CHARACTERIZATION OF DUCTILE FRACTURE IN WROUGHT STEELS AND WELDMENTS

by

E. P. Cox

F. V. Lawrence, Jr.

G. M. Sinclair

ABSTRACT

Collapse stresses of flawed structural steels were predicted by a two failure criterion model based on plasticity limit load theory and linear elastic fracture mechanics. The fracture behavior of wrought steel specimens could be characterized by either the limit load (LL) or fracture toughness (FT) failure criterion. The controlling failure criterion depended on the tensile strength (S_u), fracture toughness (K_c), and section size (W); or more explicitly, on the magnitude of $K_c/S_u\sqrt{W}$. Low values of $K_c/S_u\sqrt{W}$ resulted in FT controlled fracture; whereas, larger $K_c/S_u\sqrt{W}$ resulted in LL controlled fracture. The boundary separating the two failure criteria was dependent on geometry and crack length.

The two failure criteria model was extended to characterize the fracture behavior of A514/E110 structural steel weldments containing incomplete joint penetration discontinuities. A514/E110 weldments had large $K_c/S_u\sqrt{W}$ values; consequently, the LL failure criterion characterized the fracture behavior of those weldments containing flaw widths greater than a certain width, 2a". Flaw widths smaller than 2a" resulted in collapse stresses approximately equal to the tensile strength of the base metal, and flaw widths less than another size, 2 a' resulted in base metal fractures. The flaw widths 2a' and 2a" depended on the degree of weld metal overmatching. Deformations at collapse were predicted for flaw widths greater than 2a" by an expression which included the J-integral fracture toughness and the LL failure criterion.

The proposed two failure criteria model did not include corrections for subcritical crack extension or crack-tip plasticity. When subcritical crack extension was considered, one of three possibilities resulted depending on the tearing modulus (T) and the body's dimensions: (1) there was no effect, (2) the controlling failure criterion changed from LL to FT, or (3) fracture occurred by stable tearing. Incorporating small-scale plastic zone corrections into the model resulted in a slight increase in the $K_c/S_u\sqrt{W}$ boundary separating LL from FT controlled fracture behavior.

A Report of the

FRACTURE CONTROL PROGRAM

College of Engineering, University of Illinois
Urbana, Illinois 61801

June 1978

ACKNOWLEDGEMENT

The authors wish to thank the Fracture Control Program for supporting this study in its later stages. The investigation was conducted using the H. F. Moore Fracture Laboratory in the Department of Theoretical and Applied Mechanics and the Structural Research Laboratory of the Department of Civil Engineering.

The authors wish to thank Professor H. T. Corten of the Theoretical and Applied Mechanics Department for many helpful criticisms and useful discussions.

TABLE OF CONTENTS

TABLE OF CONTENTS (Cont'd.)

LIST OF SYMBOLS

a	Crack width or length
Δa	Change in crack length
B	Specimen thickness
b	Uncracked ligament
D	Gage length
d	Span distance of bend specimen
E	Young's modulus
e_f	Strain at fracture
e_m	Strain at maximum load
F	Geometrical factor = $f(a/W)$
G_{Ic}	Critical strain energy release rate in plane strain
J	Value of the J-integral
J_{Ic}	Value of J at the onset of crack extension in plane strain
J_m	Value of J at maximum load
K	Stress intensity factor
ΔK	Range in K during cyclic loading
K_{Ic}	Critical value of K in plane strain
L	Specimen length
P	Specimen load
P_m	Maximum load (collapse load)
P_K	Collapse stress predicted by the fracture toughness failure criterion
P_L	Collapse stress predicted by the limit load failure criterion
r	Crack length plastic zone adjustment factor
S	Gross section stress
S_m	Gross section collapse stress (at maximum load)

LIST OF SYMBOLS (Cont'd.)

S_m^K	Collapse stress predicted by linear elastic fracture mechanics
S_m^M	Collapse stress predicted by the von Mises value of the limit load
S_m^T	Collapse stress predicted by the Tresca value of the limit load failure criterion
S_o	Tensile flow stress
S_y	Uniaxial yield strength
T	Tearing modulus
U	Potential energy
W	Specimen width
Y	Compliance function - F(a/W)
β	Work hardening factor for weldments
γ	Number of crack tips
δ	Deformation in gage length
δ_m	Deformation at maximum load (collapse)
ν	Poisson's ratio
τ	Shear stress
τ_o	Shear flow stress

1. INTRODUCTION

1.1 Statement of the Problem

Linear elastic fracture mechanics (LEFM) is the accepted means for characterizing fracture of brittle materials. Brittle fractures occur with negligible plastic deformation and at loads (or stresses) well below the yield strength of the material. The ductile materials commonly used in engineering applications usually fracture at loads beyond the yield strength and then, only after extensive plastic deformation has occurred. Fracture loads of these high toughness materials often cannot be successfully predicted by LEFM for the section sizes in common usage.

Attempts to characterize ductile, post-yield fractures using elastic-plastic fracture mechanics analyses have met with varying degrees of success. One of the most promising of the elastic-plastic analyses is the J-integral proposed by Rice [1].* Experimental results have demonstrated that the J-integral can be used to measure the plane strain fracture toughness of ductile materials undergoing elastic-plastic deformation [2, 3]. The J-integral, therefore, is believed by many to provide a single parameter characterization of post-yield fracture. The J-integral has recently been investigated as a method of characterizing stable crack extension in ductile materials. Crack extension by stable tearing has been proposed by Paris et al. [4] to be dependent on a tearing modulus of the material which is determined from a J-integral crack extension resistance (R) curve. Crack extension by stable tearing is believed to proceed until the crack becomes unstable and rapid fracture commences.

---

*The bracketed numbers correspond to references listed at the end of the text.

Investigations by Lawrence and Cox [5, 6, 7, 8] and Dowling and Townley [9] have shown that ductile fracture can be characterized using a two criteria approach based on fracture mechanics and plastic limit load analyses. The fracture toughness (FT) failure criterion states that fracture will occur whenever the crack tip stress intensity exceeds the material's fracture toughness. The limit load (LL) failure criterion states that fracture (or collapse) will occur when the load on the uncracked ligament reaches the limit load of the body. The limit load is the maximum load that a body can sustain without undergoing unlimited plastic deformation. The maximum load or collapse stress that the body can support is the lower value predicted by the two failure criteria.

This investigation will explore the feasibility of characterizing ductile fractures in a variety of steels using the two failure criteria model. Experimental data from wrought steel specimens containing planar, through-thickness cracks will be compared with the collapse loads predicted using the two criteria characterization of fracture. The two criteria model will then be applied to structural steel weldments containing through-thickness, planar flaws. Before presenting these experimental results, however, a discussion of LEFM, J-integral, stable tearing, and limit load theories will be presented.

1.2 Linear Elastic Fracture Mechanics (LEFM)

Notches and cracks introduce severe stress concentrations in stressed bodies. The stress magnitude near a sharp crack in an elastic body depends upon the stress intensity factor (K):

$$K = YS(\pi a)^{\frac{1}{2}} \qquad (1)$$

where: Y = a geometry related factor

S = the externally applied stress

a = the half crack length

Fracture occurs in elastic bodies under plane strain conditions whenever K attains the critical value necessary for crack extension (K_{Ic}). The value of K_{Ic} is referred to as the fracture toughness of the material. This value of K can also be derived from the critical strain energy release rate (G_{Ic}) which, in turn, may be determined by considering that the release of elastic potential energy during crack extension is equal to the work necessary to form two crack surfaces. For plane strain, the relationship between K_{Ic} and G_{Ic} is:

$$K_{Ic}^2 = \frac{EG_{Ic}}{1 - \nu^2} \qquad (2)$$

where: E = Young's modulus

ν = Poisson's ratio

The use of LEFM to predict the fracture loads or fracture crack lengths in brittle materials is well established and a standard ASTM test method [10] for measuring K_{Ic} has been defined.

1.3 Post-Yield Fracture Mechanics

Linear elastic fracture mechanics is applicable to ductile, high toughness materials only when the section sizes are so large that any plastically deformed region is small compared to the thickness and crack length [11]. The section sizes normally used in engineering applications permit large scale plastic deformation to occur prior to fracture and the fracture loads (or stresses) are generally well above the yield strength of the material.

McClintock and Irwin [12] developed a technique for extending LEFM for small-scale, crack-tip plastic deformation. For this case, the crack length used in the LEFM analysis is increased so as to reflect the size of the crack-tip plastic zone by adding the radius of the plastic zone (r) to the actual crack length. The radius of the plane stress plastic-zone adjustment was estimated by the equation:

$$r = \frac{1}{2\pi}\left(\frac{K_{Ic}}{S_y}\right)^2 \tag{3}$$

and for plane strain:

$$r = \frac{1}{6\pi}\left(\frac{K_{Ic}}{S_y}\right)^2 \tag{4}$$

where: S_y = the uniaxial yield strength

This extension of LEFM analyses breaks down as the plastic zone increases and becomes large in comparison to the crack length and body dimensions. To characterize these latter post-yield fractures, more complex elastic-plastic fracture mechanics analyses have been proposed. One widely used elastic-plastic analysis is the J-integral. The J-integral is a path independent integral equation proposed by Rice [1] for non-linear elastic materials:

$$J = \int_{\Gamma}\left[\bar{w}dy - \vec{T}\cdot\frac{\delta\vec{u}_i}{\delta x}\right] ds \tag{5}$$

where: Γ = any contour surrounding the crack tip in a counterclockwise direction

$\bar{w}$ = the strain energy density = $\int_0^{\varepsilon_{mn}} \sigma_{ij}\, d\varepsilon_{ij}$

$\vec{T}$ = the tractions on the integration path, $\Gamma = \sigma_{ij}\,\hat{n}_j$

$\hat{n}_j$ = a normal vector to Γ

$\vec{u}_i$ = a displacement vector

ds = an increment of length along Γ

The J-integral concept is similar to the G_{Ic} criterion for fracture; i.e. J may be considered to be a measure of the difference in potential energy between two identically loaded bodies having slightly different crack lengths. The relationship between potential energy and crack length is not readily apparent from an inspection of Eq. 5, however, Rice [13] has shown that the J-integral can also be expressed by the equation:

$$J = \frac{1}{B}\frac{\partial U}{\partial(\gamma a)} \tag{6}$$

where:

U = the potential energy

B = the specimen thickness

γ = the number of crack tips

a = the crack length

The development of the J-integral was based on non-linear elastic material behavior, but J is also believed to be applicable to elastic-plastic behavior [2]. Consequently, the critical value of J for plane strain conditions (J_{Ic}) is equivalent to G_{Ic} and can be transformed into a stress intensity factor by the equation:

$$K_{Ic}^2 = \frac{EG_{Ic}}{1-\nu^2} = \frac{EJ_{Ic}}{1-\nu^2} \tag{7}$$

Experiments conducted by Begley and Landes [2, 3] and Sailors [14] have shown that the fracture toughness measured from small specimen J-integral tests is the same as the fracture toughness measured using large K_{Ic} specimens.

The first J-integral measurements required tests of several specimens having slightly different crack lengths from which values of J were graphically determined. A subsequent analysis of the J-integral by Rice et al. [15] produced a method of measuring J using a single specimen. This single-specimen method was used to measure the critical values of J in both the wrought and welded steel specimens considered in this investigation. Fracture loads predicted using Eqs. 1 and 7 tend to be unconservative and often exceed the material's tensile strength. Consequently, alternative methods of characterizing post-yield fracture behavior are needed.

1.4 Ductile Tearing

Slow, stable crack growth in structural materials by tearing has recently been studied by Paris et al. [4]. A tearing modulus (T) based on J-integral crack-extension resistance (R) curves was proposed as a measure of a material's stable tearing properties. A typical J-integral R-curve is shown in Fig. 1. As can be seen, the first amounts of crack extension are the result of the crack tip blunting (which is proportional to J):

$$\Delta a \simeq \frac{1}{2} \frac{J}{S_o} \tag{8}$$

where: S_o = the tensile flow stress

Beyond a certain value of J (J_{Ic}), however, stable crack extension occurs as indicated by the curve marked "Stable Tearing." The slope of this curve is used to calculate the tearing modulus of a material using the expression:

$$T = \frac{dJ}{da} \cdot \frac{E}{S_o^2} \tag{9}$$

where: E = Young's modulus

S_o = the tensile flow stress

The tearing modulus (Eq. 9) is a temperature independent constant for a given material provided stable tearing is the mode of crack extension. Paris et al. have indicated that crack extension by stable tearing is dependent on both the geometry and the dimensions of the body. Final fracture by unstable crack extension was proposed to occur whenever T was less than certain body dimensions for a given geometry.

1.5 Limit Load Analyses

The limit load is the maximum load that a body can withstand without undergoing unlimited plastic deformation or fracture. Limit load theory was first developed for a perfectly plastic continuum by Drucker, Prager and Greenberg [16]. Determination of the exact limit load expression for an engineering component is generally not possible because the stresses and strains in a body undergoing plastic deformation are usually not known. The exact limit load solution requires that the stress-strain relations, the strain-displacement relations, the equilibrium equations and the yield criterion be satisfied simultaneously. For this reason, upper and lower bound approximations are used to treat difficult limit load problems. Theorems have been established for calculating upper and lower bounds based on rigid-plastic material behavior [17].

The lower bound theorem states that a body will not collapse or will be just at the point of collapse if an equilibrium distribution of stress

can be found which balances the applied load (equilibrium) and is below or at yield at all points in the body. The lower bound theorem provides a method of determining the limit load without knowing the exact stress distribution.

The upper bound theorem states that the body will collapse or will have collapsed previously whenever a deformation mode can be found in which the rate of work done by the external forces equals or exceeds the rate of internal energy dissipation. More specifically, an upper bound for the limit load is attained when the body is loaded such that displacements can be found (with no change in volume for metals) satisfying the displacement boundary conditions and such that the resulting plastic work done throughout the body is less than the work done by the external loads acting through the assumed displacements. The assumed displacements need not be the actual displacements.

The difference in collapse loads predicted using the upper and the lower bound limit load theorems is an indication of the error present in applying these approximations to a problem. The exact limit load solution provides coincident upper and lower bounds.

The limit load theorems assume a continuum which exhibits elastic-perfectly plastic or rigid-plastic stress-strain behavior. Elastic-perfectly plastic stress-strain behavior is illustrated in Fig. 2 by the curve labeled "idealized material." This idealized behavior has a tensile flow stress (S_0) which was equated to the tensile strength (S_u) of the real material. Limit load solutions based on the ultimate strength of a material have the potential of being unconservative, hence a lower flow stress should be chosen for design purposes.

The design of structures which may contain cracks must also consider the multi-axial state of stress at the crack tip. The onset of plastic deformation in a multiaxial stress state occurs only when the magnitude of the stresses meet the requirements of a yield criterion. For uniaxial tension, plastic deformation begins when the applied stress is equal to the yield or flow stress, i.e. when $S = S_y$. However, for multiaxial stresses, the onset of plastic deformation occurs when a yield criterion is satisfied, and for isotropic materials, the yield criterion depends on the invariants of the stress tensor.

The Tresca yield criterion states that plastic deformation begins when the maximum shear stress, τ_{max}, is equal to the flow stress in shear. The maximum shear stress is equal to half the difference between the maximum and minimum principal stresses:

$$\tau_{max} = \frac{\sigma_1 - \sigma_3}{2} \tag{10}$$

where σ_1, σ_2 and σ_3 are the principal stresses in decreasing magnitude. As previously stated, plastic deformation in uniaxial tension ($S = \sigma_1$, $\sigma_2 = \sigma_3 = 0$) occurs when $\sigma_1 = S_y$, consequently, the shear flow stress τ_o is given by:

$$\tau_o = \tau_{max} = \frac{S_y}{2} = \frac{S_o}{2} \tag{11}$$

For the idealized material behavior shown in Fig. 2, plastic deformation, as determined by the Tresca yield criterion, will commence when:

$$\tau_o = \frac{S_o}{2} = \frac{S_u}{2} \tag{12}$$

A second yield criterion, known as the von Mises yield criterion, states that plastic deformation will occur whenever:

$$6\tau_o^2 = (\sigma_1 - \sigma_2)^2 + (\sigma_2 - \sigma_3)^2 + (\sigma_3 - \sigma_1)^2 \qquad (13)$$

For uniaxial tension ($\sigma_1 = S_o$, $\sigma_2 = \sigma_3 = 0$) plastic deformation occurs whenever

$$\tau_o = \frac{S_o}{\sqrt{3}} = \frac{S_u}{\sqrt{3}} \qquad (14)$$

where $S_o = S_u$ for the idealized stress-strain behavior shown in Fig. 2.

The Tresca and von Mises yield criteria will be used extensively in calculating the limit loads(or collapse stresses) of the specimen configurations used in this investigation. The range of collapse loads predicted by these yield criteria will be compared with experimental values.

1.6 Two Criteria Characterization of Ductile Fracture

A two failure criteria characterization of ductile fracture has recently been considered by many investigators including Lawrence and Cox [5, 6, 7, 8] and Dowling and Townley [9]. The concept is simple: failure occurs at the lower of the two loads (or stresses) predicted by the FT and LL failure criteria. The behavior of full-size structures can be readily determined based on their geometry and the results of small specimen tensile and fracture toughness tests. This two failure criteria model is easily adapted to design and engineering.

The fracture toughness (FT) failure criterion is derived from Eq. 1. Fracture by this failure criterion occurs only when crack tip plastic deformation is small and when the stress intensity factor (K) attains the critical value, K_{Ic} (for plane strain), which is the fracture toughness of the material. The fracture (collapse) stress for a given geometry and fracture toughness is consequently calculated using a rearranged version of Eq. 1:

$$S_m^K = \frac{K_{Ic}}{Y\sqrt{\pi a}} \tag{15}$$

where: S_m^K = the collapse stress

Y = a geometry related factor

The fracture toughness, K_{Ic}, must be determined for each material and Y must be evaluated for each geometry.

The limit load failure criterion is used to determine the collapse stress at which the plastic deformation is not contained in the body. The expression for the LL failure criterion (in terms of gross section stress) is:

$$S_m = 2\tau_o F \tag{16}$$

where: S_m = the collapse stress

F = a geometry related factor

The collapse stress for the idealized stress-strain behavior shown in Fig. 2 can be determined using either the von Mises or Tresca yield criteria given in Eqs. 14 and 12, respectively. For the von Mises yield criterion, in the presence of biaxial tension ($\sigma_2 = \frac{1}{2}\sigma_1$, $\sigma_3 = 0$) collapse occurs when:

$$2\tau_o = \frac{2}{\sqrt{3}} S_o = \frac{2}{\sqrt{3}} S_u \tag{17}$$

and the LL collapse stress is given by:

$$S_m^M = \frac{2}{\sqrt{3}} S_u F \tag{18}$$

As will be shown, the two criteria characterization of ductile fracture is a concept that can be applied to many practical problems including weldments. For the present, however, consider a homogeneous continuum having the idealized stress-strain behavior shown in Fig. 2. The two criteria model

of ductile fracture behavior will be illustrated for the center-crack tension (CCT) and compact specimen (CS) geometries. Three-point bend (3PB) and four-point bend (4PB) specimen geometries were also used in the wrought steel tests. The collapse loads predicted using the LL and FT failure criteria for these specimen geometries are discussed in Appendix A.

The limit load for the CCT specimen geometry, was determined by McClintock [18]:

$$P_L = 2\tau_o B(2W - 2a) \tag{19}$$

where: B = the specimen thickness

2W = the specimen width

By rearranging Eq. 19, the gross section stress at collapse is given by:

$$S_m = \frac{P_m}{2BW} = 2\tau_o\left(1 - \frac{a}{W}\right) \tag{20}$$

which becomes a failure criterion when the shear flow stress at fracture is replaced by either the von Mises or Tresca yield criteria given by Eqs. 17 and 12, respectively. That is, the collapse stress predicted using the von Mises yield criterion is:

$$S_m^M = \frac{2}{\sqrt{3}} S_u \; 1 - \frac{a}{W} \tag{21}$$

and similarly, the collapse stress using the Tresca yield criterion is:

$$S_m^T = S_u\left(1 - \frac{a}{W}\right) \tag{22}$$

The curves corresponding to the von Mises and Tresca values of collapse stress are shown as solid lines in Fig. 3. The region between these lines is labeled "Limit Load Failure Criterion" to illustrate the range in collapse stress predicted by the LL failure criterion.

The collapse stress curve predicted by the fracture toughness failure criterion for the center-crack specimen geometry is given by the equation:

$$S_m^K = \frac{K_{Ic}}{(\pi a)^{\frac{1}{2}}\left(\sec \frac{\pi a}{2W}\right)^{\frac{1}{2}}} \qquad (23)$$

This curve in Fig. 3 is labeled "Fracture Toughness Failure Criterion" and is shown crossing the region labeled "Limit Load Failure Criterion." The value of S_m^K is dependent on K_{Ic}, a and W, whereas S_m^M and S_m^T are dependent on S_u, a and W. Consequently, as S_u, W and K_{Ic} change, the values of S_m also change and the intersection between the LL and FT failure criteria may be eliminated completely so that only one failure criterion prevails. For the case where an intersection does occur, as shown in Fig. 3, the collapse stress will be predicted by the failure criterion with the lower stress. Here the LL failure criterion characterizes fracture for the smaller values of a/W and the FT failure criterion characterizes fracture for the larger values of a/W. The transition from one failure criterion to another occurs (approximately) whenever $S_m^T = S_m^K$.

The second illustration of the two failure criteria characterization of ductile fracture will use the compact specimen geometry shown in Fig. 4. Since an exact limit load solution does not exist, upper and lower bound solutions determined by Rice [19] and Ewing and Richards [20], respectively, are shown. The von Mises and Tresca yield criteria are indicated on both the upper and lower bound solutions. To be conservative, the lower bound LL solution of Ewing and Richards was chosen and will be used to analyze the wrought steel results presented later. The Ewing and Richards LL expression is:

$$P_L = \{\sqrt{2}[1 + \frac{a}{W}]^{\frac{1}{2}} - [1 + \frac{a}{W}]\} (2\tau_o) BW \qquad (24)$$

which, when rearranged, and the von Mises yield criterion (Eq. 17) inserted for the flow stress, the collapse load is:

$$\frac{P_L}{BW} = \{\sqrt{2}[1 + \frac{a}{W}]^{\frac{1}{2}} - [1 + \frac{a}{W}]\} \cdot \frac{2}{\sqrt{3}} S_u \qquad (25)$$

and for the Tresca yield criterion (Eq. 12) the collapse load is:

$$\frac{P_L}{BW} = \{\sqrt{2}[1 + \frac{a}{W}]^{\frac{1}{2}} - [1 + \frac{a}{W}]\} \cdot S_u \qquad (26)$$

When the FT failure criterion is used to predict the collapse load in a compact specimen, the collapse load is given by:

$$\frac{P_K}{BW} = \frac{K_{Ic}}{Y\sqrt{W}} \qquad (27)$$

where Y is the compliance function for a compact specimen given in the ASTM standard K_{Ic} test method [10].

The relationship between the two failure criteria for the compact specimen is shown in Fig. 4. Whenever the LL failure criterion predicts a lower collapse load, it will dominate fracture as is shown for the smaller b/W values. Similarly, fracture will be characterized by the FT failure criterion when it predicts the lower load value; this is indicated for the larger b/W values. The intersection and relative locations of the two failure criteria are dependent on the specimen dimensions and the material's tensile strength and fracture toughness.

2. CHARACTERIZATION OF DUCTILE FRACTURE IN WROUGHT STEELS

2.1 Background

The feasibility of using limit load and fracture toughness failure criteria to characterize the fracture behavior of wrought steels will be demonstrated in this section. Experimental data [2, 3, 14, 21, 22] for a wide variety of structural steels of various strengths and fracture toughnesses have been collected and reanalyzed. These data were obtained from J-integral fracture toughness tests using compact (CS), three-point bend (3PB) and four-point bend (4PB) specimens. Only experimental results reporting both the collapse loads (maximum load values) and J-integral fracture toughness values were reanalyzed. The critical K values determined from the J-integral tests have been denoted K_c to distinguish these values from the ASTM E399 [10] fracture toughness K_{Ic}.

The steels and the specimen geometries considered were:

Steel	Specimen Type	S_y	Reference
1E170	CS	41	14
A533B	CS, 3PB	72	2, 3
1EAEG	CS	106	14
1EAFD	CS	161	14
Ni-Cr-Mo-V	3PB	124	2, 3
AISI 4340	4PB	113	21
A514F	4PB	110	22
AISI 4340	4PB	174	21

These steels range in yield strength from 41 ksi for the hot-rolled 1E170 steel to 174 ksi for the quenched and tempered 4340 steel. The strength levels and other pertinent data are given for each steel in Tables 1-8.

2.2 Results

Using the format of Figs. 3 and 4, the reanalyzed results have been grouped by specimen geometry. For the compact specimen geometry, the collapse loads were divided by the specimen width and thickness and plotted

versus b/W in Figs. 5-8. The collapse loads of the three- and four-point bend specimens were divided by thickness and plotted versus b. These results are shown in Figs. 9 and 10 and 11 through 14, respectively. As in Figs. 3 and 4, the collapse loads predicted by the LL and FT failure criterion are shown on each of the figures for comparison with the experimental results. In addition, limit loads have been determined for the flow stresses equal to the uniaxial yield strengths and have been plotted on the figures. These yield strength limit loads indicate the onset of net section plastic deformation and illustrate the effect of work hardening on the LL failure criterion.

The sets of data which conform to the LL failure criterion are shown in Figs. 5, 6, 9, 10, 11, 12 and 13. The experimental collapse loads generally lie between the von Mises and Tresca LL curves. The Tresca yield criterion is slightly conservative. Very conservative LL collapse load predictions result for the lower strength steels when the flow stress, S_o, is equated to the yield strength, S_y. However, for those materials that do not work harden appreciably, i.e. the higher strength quenched and tempered steels, there is little difference between the limit loads calculated using either the yield or tensile strengths. Collapse loads that agreed with the FT failure criterion are shown in Figs. 7 and 8.

The effect of section size is illustrated in Figs. 6 and 14. The collapse loads in Fig. 6 agree with the collapse loads predicted by the LL failure criterion for the specimen dimensions tested. The interesting point, though, is that the collapse load curves predicted by the FT failure criterion decrease as the section size increases. Continuing to increase the section size would result in an intersection between the two failure criteria. This phenomenon occurs for the high strength 4340 steel specimens (Fig. 14).

Collapse loads for the 4340 steel are characterized by the LL failure criterion for the smaller values of b but the larger values of b result in collapse loads that agree with those predicted by the FT failure criterion.

2.3 Data Analysis and Discussion

The experimental results shown in Figs. 5-14 illustrate that ductile fracture can be characterized by a two failure criteria model. The experimental data always agreed with the lower of the two collapse loads predicted by the two failure criteria model.

Data which agreed with the limit load failure criterion were between the values predicted using the von Mises and Tresca yield criteria. Limit loads determined using a flow stress equal to the yield strength showed no consistent relationship with the measured collapse loads. Consequently, design loads based on a limit load approach should be calculated using a flow stress equal to the ultimate strength.

The FT failure criterion characterized the fracture behavior of the higher strength steels but showed a tendency, as seen in Fig. 6, to control the fracture of the lower strength steels having thick sections. The collapse loads of specimens controlled by the FT failure criterion were less than the loads necessary to cause net section yielding.

A transition from one failure criterion to another (Fig. 14) occurs only for certain combinations of specimen dimensions, tensile strength, fracture toughness and crack length (or uncracked ligament). This crack length can be determined by equating the LL and FT collapse loads given by Eqs. 21, 22 and 23:

$$S_m^M \text{ or } S_m^T = S_m^K \tag{28}$$

which, for the CCT geometry becomes:

$$S_u\left(1 - \frac{a}{W}\right) = \frac{K_c}{\left(\pi a \sec \frac{\pi a}{2W}\right)^{\frac{1}{2}}} \tag{29}$$

for the Tresca yield criterion, and

$$\frac{2}{\sqrt{3}} S_u\left(1 - \frac{a}{W}\right) = \frac{K_c}{\left(\pi a \sec \frac{\pi a}{2W}\right)^{\frac{1}{2}}} \tag{30}$$

for the von Mises yield criterion. These equations can be rearranged in terms of a/W to yield the following equation:

$$\frac{K_c}{S_u\sqrt{W}} = \left(1 - \frac{a}{W}\right)\left(\frac{\pi a}{W} \sec \frac{\pi a}{2W}\right)^{\frac{1}{2}} \tag{31}$$

for the Tresca yield criterion. The right-hand side of this equation is multiplied by $2/\sqrt{3}$ when the von Mises yield criterion is desired.

The quantity $K_c/S_u\sqrt{W}$ relates the strength, fracture toughness and section size to the controlling failure criterion. This quantity is plotted versus a/W in Fig. 15. When K_c is low and S_u is high, which corresponds to a low value of $K_c/S_u\sqrt{W}$, the fracture toughness failure criterion dominates the fracture behavior. Increasing K_c and decreasing S_u increases the value of $K_c/S_u\sqrt{W}$ into the limit load region. Crack length also affects which failure criterion controls fracture. For instance at $K_c/S_u\sqrt{W} = 0.6$, the controlling failure criterion changes from LL to FT at an a/W of approximately 0.1 and from FT back to LL at an a/W of approximately 0.85.

The relationship between $K_c/S_u\sqrt{W}$ and a/W for the 3PB specimen is shown in Fig. 16. The Tresca and von Mises curves that separate the FT controlled fracture from the LL controlled fracture region have different shapes than those seen for the center-crack tension specimen in Fig. 15. The skewed curves result from the FT and LL interactions for this geometry.

A comparison between the predicted controlling failure criterion and experimental results is made in Fig. 17 for the 3PB specimen. Unfortunately, all the data were limit load controlled failures; however, they do substantiate the existence of the limit load region predicted.

Figures 15 and 16 illustrate perhaps the most important aspect of the two failure criteria model: the possibility of an a priori characterization of fracture behavior. Once the tensile strength and fracture toughness are known, the controlling failure criterion can be determined for the geometry and section size of the body. This approach is far simpler than calculating individual FT and LL values.

3. EXTENSION OF THE TWO FAILURE CRITERIA MODEL TO WELDMENTS

3.1 Background

In the previous section, the two failure criteria model was shown to characterize accurately the fracture behavior of wrought structural steels. This chapter will demonstrate how the model can be applied to structural steel weldments and how base metal (BM) and weld metal (WM) strengths influence the fracture behavior. Since most structural steel weldments are fabricated from low strength and high fracture toughness materials, their fracture behavior is usually controlled by the LL failure criterion. The data to be discussed in this chapter will illustrate the limit load fracture behavior that is peculiar to weldments.

Weldments are heterogeneous structural elements composed of three microstructural regions: base metal (BM), weld metal (WM), and heat affected zone. Each of these regions have a different yield strength, tensile strength, and fracture toughness. The weld metal usually has a higher strength (tensile and yield) than the base metal and is said to be "overmatched." The amount by which the weld metal strength exceeds the base metal strength is the "degree of overmatching." For a given base metal, the degree of overmatching is influenced by several parameters such as weld metal chemistry, welding process, preheat and interpass temperature, and heat input.

3.2 Ductile Fracture of Weldments - Theory

Very small flaws in tough, overmatched weld metal ($S_{yWM} > S_{uBM}$) are of minor consequence, since failure will occur in the base metal at loads less than those required for plastic deformation in the weld metal net section. The load carrying capacity of these weldments is thus limited by the tensile

strength of the base metal as illustrated by Region A in Fig. 18. The maximum flaw width (a'/W) that will result in base metal controlled fracture can be estimated by equating the collapse stress predicted by the Tresca value of the LL failure criterion to the base metal tensile strength:

$$S_{uBM} = S_{uWM}\left(1 - \frac{a}{W}\right) \tag{32}$$

When solved for a'/W, this equation becomes

$$\frac{a'}{W} = 1 - \frac{S_{uBM}}{S_{uWM}} \tag{33}$$

Flaw widths greater than a'/W cause both the base and weld metals to plastically deform, but final fracture occurs in the flawed weld metal. Because the lower strength base metal is part of the fracture process, the collapse loads are limited by the base metal tensile strength. The tensile behavior of these flawed weldments is shown as Region B in Fig. 18.

Beyond a certain flaw size (a"/W), fracture occurs in the flawed weld metal at stresses less than the base metal yield strength. Weldments containing these larger flaws fail in the weld metal and exhibit tensile behavior in accordance with the LL failure criterion, as shown by Region C in Fig. 18. The value of a"/W can be estimated by equating the Tresca LL failure criterion to the base metal yield strength:

$$S_{yBM} = S_{uWM}\left(1 - \frac{a}{W}\right) \tag{34}$$

Solving for a"/W gives the equation:

$$\frac{a''}{W} = 1 - \frac{S_{yBM}}{S_{uWM}} \tag{35}$$

The relative values of a'/W and a"/W shown in Fig. 18 are dependent on the tensile and yield strength of both the base and weld metals, that is, the degree of overmatching. The curves shown in Fig. 19 illustrate the effect that the degree of overmatching (S_{yBM}/S_{uWM}) has on a'/W and a"/W and how overmatching affects the extent of Regions A, B and C shown in Fig. 18.

The combinations of relative flaw width and overmatching that causes fracture in the base metal prior to yielding of the weld metal net section are contained within Region A. Since the fracture is completely controlled by the unflawed base metal, large amounts of plastic deformation occur; and the stress at fracture is approximately equal to the base metal tensile strength. Region A represents high toughness joints for which weld metal flaws are benign under static loading.

The relative flaw widths and degree of overmatching included in Region B of Fig. 19 result in fractures in which both the base and weld metals deform plastically. The joint toughness is still high because large amounts of plastic work are expended in deforming the base metal. The extent of Region B varies with the amount of work hardening (β) available in both the base and weld metals. The value of β is defined as:

$$\beta = \frac{S_{uBM}}{S_{yBM}} \cdot \frac{S_{uWM}}{S_{yWM}} \tag{36}$$

The boundary separating Region B from Region A is given by the equation:

$$\frac{a'}{W} = 1 - \beta \frac{S_{yBM}}{S_{uWM}} \tag{37}$$

and the boundary between Region B and Region C is expressed by:

$$\frac{a''}{W} = 1 - \frac{S_{yBM}}{S_{uWM}} \qquad (38)$$

The extent of Region B, therefore, is dependent on the degree of overmatching and on the work hardening of the base and weld metals. That is, Region B diminishes as the degree of overmatching (S_{yBM}/S_{uWM}) approaches zero or when both the base and weld metal do not work harden ($\beta = 1.0$).

Referring to Fig. 18, the fracture behavior of high toughness weldments (large $K_c/S_u\sqrt{W}$) was divided into three regions separated by the transition flaw widths a'/W and a"/W. A weldment containing weld metal flaw widths less than a"/W will reach a collapse stress (S_m) approximately equal to the base metal tensile strength. Flaw widths greater than a"/W cause a reduction in S_m as predicted by the limit load failure criterion. Fracture toughness controlled failures may occur for very large a/W at stresses predicted by the curve labeled S_m^K, as previously discussed in Chapter 2.

3.3 Ductile Fracture of Weldments - Experimental Results

3.3.1 Specimen Preparation and Testing

The effect of weld metal discontinuities on the fracture behavior of a structural steel was investigated using ASTM A514 grade F (ASTM specification for high-yield strength, quenched and tempered alloy steel plate, suitable for welding) base metal welded with E110-S bare wire electrode. Chemical compositions of both the base metal and electrode are given in Table 9. Weldments were fabricated with internal full-length, incomplete joint penetration (IJP) discontinuities which resulted in the CCT specimen geometry shown in Fig. 20. An enlarged view of the IJP test section is shown in Fig. 21.

The test specimens were butt welded together using a 60° double V-groove joint preparation and a variable land (root face) to control the width (2a)

of the IJP. The welding parameters used to fabricate the specimens were:

Welding process	Gas Metal Arc (GMA)
Voltage	28-30 v
Current	285-295 amps
Preheat and interpass temperature	200°F
Shielding gas composition	98% AR-2% O_2

The torch travel speed was varied to produce the desired heat input in the weld metal. Most of the specimens were fabricated with a single 30 kJ/in. weld pass per side. Other specimens were similarly fabricated except that welding heat inputs of 20, 50 and 90 kJ/in. were used. Weld metal tensile and yield strengths are shown versus heat input in Fig. 22.

Most of the specimens contained as-welded IJP discontinuities and were tested in tension after fabrication. Other specimens were tested after the IJP was fatigue sharpened; some specimens were fabricated with altered V-groove angles or inclined IJP's. A complete discussion of the test results obtained from these specimens is given in Ref. 5. In general, altering the IJP had little effect on the tensile behavior.

The load and deformation responses were recorded during testing. These were used to determine the weldment yield strength (S_y), collapse stress (S_m), collapse strain (e_m) and the value of J at maximum load (J_m).

3.3.2 Experimental Results

The experimental results of the welds containing varying length IJP discontinuities are presented in Tables 10-14. Values of e_m, J_m and S_m are plotted in Figs. 23-26 for welding heat inputs of 20, 30, 50 and 90 kJ/in., respectively, and the S_m data are compared with the collapse stresses predicted by the Tresca and von Mises values of the LL failure criterion (Eqs. 21 and 22). The transition flaw sizes 2a' and 2a" were determined using Eqs. 33 and 35.

Most of the specimens were welded with a 30 kJ/in. heat input; consequently, the best comparison between the theorized tensile behavior (see Fig. 18), and experimental results is shown for this heat input in Fig. 24. Examining first the e_m data, it can be seen that e_m reaches its lowest value at flaw widths greater than 2a". As 2a decreases, e_m increases. A similar response is seen in the J_m data. The lowest values of J_m occur for values of 2a greater than 2a". All plastic deformation in these specimens was confined to the uncracked ligaments which is a necessary requirement for a valid J-integral measurement using the single specimen method [15]. The values of J_m measured in specimens containing 2a less than 2a" are not valid because base metal plastic deformation not associated with the crack tips was included in the J measurement. Collapse stress (S_m) data agreed quite well with the tensile behavior predicted by the LL failure criterion. The experimental results for the 20, 50 and 90 kJ/in. heat input specimens are shown in Figs. 23, 25 and 26. With the exception of specimen 6125 (50 kJ/in.), which contained secondary discontinuities, the experimental S_m values lie within the range predicted by the Tresca and von Mises values of the LL failure criterion.

The J-integral fracture toughness varied for each of the heat inputs tested. Average valid J_m values measured for each heat input are:

Heat Input	Average Valid J_m Value
20 kJ/in.	1.17 kip/in.
30	1.43
50	1.15
90	1.14

For the CCT specimen having the dimensions shown in Fig. 20, the weld metal values of $K_c/S_u\sqrt{W}$ ranged from 2.29 to 2.74. Referring to Fig. 15, it can be seen that the test specimens were well within the region where the limit load failure criterion dominates the fracture behavior.

The calculated value of 2a' (base metal dominated fracture) for the 30 kJ/in. heat input welds was 0.032 in. This was the only 2a' that could be calculated because the S_{yWM}'s for the other heat inputs were all less than S_{uBM}. Consequently, only the 30 kJ/in. heat input specimens exhibited base metal-controlled tensile behavior corresponding to Region A in Fig. 18.

Values of 2a" (the minimum flaw width corresponding to limit load controlled fracture in the weld metal) were calculated for each weldment. The 2a" values, which are shown in Figs. 23-26, were calculated using Eq. 35:

Heat Input	S_{yBM}/S_{uWM}	2a"
20 kJ/in.	0.79	0.146 in.
30	0.81	0.135
50	0.84	0.114
90	0.99	0.007

The 2a" transition flaw width decreased as the degree of overmatching decreased. The calculated 2a" value for the 90 kJ/in. heat input specimens (see Fig. 26) was very small ($\sim$0.007 in.) which meant that the tensile behavior was controlled by the limit load failure criterion for nearly all flaw widths. Only flaw widths less than approximately 0.007 in. would cause the base metal to participate in the fracture process; otherwise, fracture is completely controlled by the weld metal net section.

3.4 Use of the J-Integral to Predict the Deformation at Collapse

Valid J-integral fracture toughness measurements were obtained from the test specimens containing IJP flaws greater than a"/W. The fracture toughness, however, was not useful for predicting the collapse stress of the test specimen, as shown in Fig. 27, because the tensile behavior was controlled by the LL failure criterion.

Materials that fail by the LL failure criterion also have measurable values of fracture toughness. In these failures, the collapse stress is controlled by the LL failure criterion; but the amount of corresponding plastic deformation may be controlled by a critical value of plane-strain ductility. For LL controlled failures, the J-integral fracture toughness is essentially a measurement of the plastic work, i.e. the area under the load-deformation curve. Consequently, if the limit load and fracture toughness are known, it should be possible to determine the deformation at collapse.

The A514F/E110 weldments discussed previously had tensile stress-strain curves that could be approximated by a rigid-plastic material behavior. The collapse stresses were predicted by Eqs. 21 or 22, depending on whether the Tresca or von Mises yield criterion was chosen. The LL failure criterion was combined with the J-integral fracture toughness to predict the deformation at collapse (maximum load), δ_m; this derivation is given in Appendix B. The value of δ_m is given by:

$$\delta_m = \frac{J_m}{S_m}\left(1 - \frac{a}{W}\right) \tag{39}$$

for a/W greater than a"/W where fracture is controlled by the LL failure criterion.

The δ_m data obtained from the as-welded, 30 kJ/in. heat input weldments are compared with the predicted δ_m in Fig. 28. The data tend to lie within the δ_m^T (Tresca yield criterion) and δ_m^M (von Mises yield criterion) curves. Good agreement occurs for 2a greater than 2a"; but the agreement is poor, as predicted, for 2a less than 2a".

4. DISCUSSION

4.1 The Two Failure Criteria Model

A model to characterize the fracture behavior of structural materials was proposed in Chapter 1. The model was based on fracture toughness and limit load predictions of the collapse load which were called the fracture toughness and limit load failure criteria. Fracture was proposed to occur at a load equal to the lower of the loads predicted by the two failure criteria as illustrated for center-crack tension and compact specimen geometries in Figs. 3 and 4.

The two failure criteria model was compared in Chapter 2 with experimental data obtained from a variety of wrought structural steels and test specimen geometries. Good agreement was shown between the experimental data and the predicted collapse loads in Figs. 5-14. The two failure criteria were then equated for a given strength and fracture toughness, and the boundary separating the limit load from the fracture toughness failure criteria was determined. For a given geometry, the controlling failure criterion was found to depend on a strength-fracture toughness-section size factor, $K_c/S_u\sqrt{W}$, and crack length, a/W, as shown in Figs. 15 and 16. These results suggested the possibility of an a priori prediction of the controlling failure criterion and a method of separating below yield strength "brittle" fracture behavior from post-yield, elastic-plastic fractures.

The quantity $K_c/S_u\sqrt{W}$ was shown in Fig. 17 to be appropriate for separating the regions controlled by the two failure criteria. Experimental data obtained from A514F/E110 weldments containing incomplete joint penetration discontinuities were analyzed in Chapter 3 using the two failure criteria model concepts. The $K_c/S_u\sqrt{W}$ value predicted limit load controlled behavior, but base metal-weld metal interactions made the fracture model more complicated,

as shown in Fig. 18. At large IJP flaw widths, the LL failure criterion predicted the collapse stress; and the combination of the limit load failure criterion and the J-integral fracture toughness was shown to predict the deformation at collapse.

The two failure criteria model has been shown to predict the collapse loads of flawed structural materials, to be useful in predicting whether the fracture behavior will be predominantly elastic or elastic-plastic, and to help predict the deformation at collapse. The model discussed has been based on two major assumptions: (1) fracture toughness failures are characterized by LEFM with negligible plastic deformation, and (2) no subcritical crack extension occurs. The following sections will discuss the effects that these assumptions have on the model.

4.2 The Effects of Subcritical Crack Extension on the Two Failure Criteria Model

Subcritical crack extension has been shown [23] to significantly affect the critical value of the J-integral. In the same study, J-integral crack-extension resistance (R) curves were observed to be geometry and section size dependent. Hence, subcritical crack extension is believed to affect the two criteria fracture model by altering the load-crack length trajectory prior to collapse. This effect is schematically illustrated for an overmatched butt weld containing a centralized, planar discontinuity in Fig. 29. Trajectory A is the stress-crack length trajectory for a flaw which does not undergo subcritical crack extension; fracture occurs by the failure criterion that trajectory A encounters first. If the material exhibits subcritical crack extension, then its stress-crack length trajectory may follow a path similar to those illustrated by the "B" curves.

The onset of subcritical crack growth occurs when the value of J at the crack tip exceeds the value of J_{Ic} [23]. The trajectory from this point until fracture occurs is dependent on the tearing behavior of the material. Final fracture occurs when the stress-crack length trajectory intersects one of the failure criteria. As seen in Fig. 29, the occurrence of subcritical crack extension can change the controlling failure criterion and, to some extent, the collapse load.

The tearing behavior of structural materials has been described in terms of a tearing modulus (T) by Paris et al. [4]. The relationship between the fracture toughness measured using the J-integral and the change in crack length is illustrated in Fig. 1 and discussed in section 1.4.

The effect of stable tearing can be incorporated into the two failure criterion model for a center-crack tension specimen since unstable limit load failure was stated to occur [4] whenever:

$$T \leq \frac{L}{W} \tag{40}$$

Using Eq. 9 and the relationship that

$$J \approx \frac{K^2}{E} \tag{41}$$

Equation 40 becomes

$$T \approx \frac{d(K^2)}{da} \cdot \frac{1}{S_o^2} \leq \frac{L}{W} \tag{42}$$

When Eq. 42 is integrated and subsequently divided by $\sqrt{W}$ the result is:

$$\frac{K}{S_o\sqrt{W}} \leq \left[\frac{L}{W} \cdot \frac{a}{W}\right]^{\frac{1}{2}} \tag{43}$$

Curves determined from Eq. 43 for various values of $\sqrt{L/W}$ are shown in Fig. 30 for the center-crack tension specimen. Subcritical crack extension precedes final fracture in the region lying above the appropriate $\sqrt{L/W}$ line, and below this line, no subcritical crack extension occurs prior to fracture. Bodies prone to subcritical crack extension follow a $K_c/S_u\sqrt{W}$ - a/W trajectory until one of the failure criteria is encountered or the crack extends across the entire specimen.

4.3 The Effects of Plastic Zone Correction on the Two Failure Criteria Model

The use of a crack tip plastic zone adjustment factor (r) was discussed in section 1.3. The adjustment factor, r, was proposed for use with small-scale crack tip plastic deformation [12].

The data shown in Figs. 5-14 indicate that accurate collapse stress predictions are possible using an uncorrected FT failure criterion. These results, however, may have been fortuitous, so the FT failure criterion was recalculated using the value of r given by Eq. 4 and these results were compared with Figs. 15 and 16. The corrected and uncorrected FT-LL boundaries are shown in Figs. 31 and 32 for the CCT and 3PB geometries, respectively.

There are two main differences between the corrected and uncorrected boundaries for the CCT geometry shown in Fig. 31. The first difference is an enlargement of the region dominated by the FT failure criterion. The plastic zone correction resulted in the ordinate of von Mises and Tresca boundaries being increased approximately 10 and 7 percent, respectively. This difference is relatively small and will have little effect on the two failure criteria model. The second difference is the prediction of a fracture toughness failure criterion band for large values of $K_c/S_u\sqrt{W}$. This

band is believed to be an artifact of the analysis resulting from large plastic zone corrections when the fracture toughness is high. Since the plastic zone correction was developed and applied for small scale yielding, large plastic zones are inappropriate.

The Irwin-McClintock plastic zone [12] is assumed to have the form of a circular cylinder at the crack tip. This assumption is not a realistic description of the crack tip plastic zone but nevertheless has been accepted and successfully used for many years.

The fracture toughness region is also expanded when the crack tip plastic zone correction is included in the fracture toughness failure criterion of the three-point bend specimen (Fig. 32). The presence of a small limit load region within the expanded, plastic zone corrected fracture toughness region is an interesting phenomenon. The large expansion of the LL-FT boundary and the presence of a central limit load region are believed to be artifacts of the plastic zone correction and therefore not representative of the real material behavior which is summarized in Fig. 17.

TABLE 1

Test Results of 1E170 Steel[a]
(Compact Specimen)

Specimen	B in.	W in.	b in.	P_m kip	P_m/B kip/in.	P_m/BW kip/in.^{2}	b/W	J_m[b] kip/in.	S_y ksi	S_u ksi
1	1.01	2.00	0.69	5.22	5.17	2.58	0.345	0.588	41	67
3			0.61	3.95	3.91	1.95	0.305	0.660		
22			0.57	3.30	3.27	1.63	0.285	0.639		
4			0.54	2.82	2.79	1.39	0.270	0.391		
5			0.46	2.45	2.43	1.21	0.230	0.483		
24			0.40	1.66	1.64	0.82	0.200	0.440		
6			0.39	1.66	1.64	0.82	0.195	0.536		
2			0.26	0.81	0.80	0.40	0.130	0.460		

a. Reference 14
b. The average value of J_m corresponds to K_{Ic} = 126 ksi$\sqrt{\text{in.}}$

TABLE 2

Test Results of A533B Steel[a]

Specimen	B in.	W in.	b in.	P_m kip	P_m/B kip/in.	P_m/BW kip/in.^{2}	b/W	J_m kip/in.	S_y ksi	S_u ksi
I. 3 Point Bend, d = 3.15, (K_{Ic} = 257 ksi$\sqrt{in.}$)										
DCF12	0.788	0.788	0.615	11.75	14.91	18.92	0.780	2.00	72	90
DCF13			0.533	8.77	11.13	14.12	0.676			
DCF14			0.470	7.05	8.95	11.36	0.596			
DCF15			0.373	4.35	5.52	7.01	0.473			
DCF16			0.295	2.80	3.55	4.51	0.374			
II. Compact Specimens-Group A (K_{Ic} = 177 ksi$\sqrt{in.}$)										
HS2175	2.00	4.00	1.998	57.00	28.50	7.13	0.500	0.95	72	90
HS2176			1.905	52.00	26.00	6.50	0.476			
HS2177			1.790	46.20	23.10	5.78	0.448			
HS2178			1.705	41.50	20.75	5.19	0.426			
III. Compact Specimens--Group B (K_{Ic} = 184 ksi$\sqrt{in.}$)										
8-4-1	1.00	2.00	0.995	15.74	15.74	7.87	0.498	1.03	72	90
8-4-2			0.942	13.85	13.85	6.93	0.471			
18-4-2			0.906	12.00	12.00	6.00	0.453			
18-4-3			0.854	10.80	10.80	5.40	0.427			
18-4-4			0.793	9.20	9.20	4.60	0.397			

a. References 2 and 3

TABLE 3

Test Results of 1EAEG Steel[a]
(Compact Specimen)

Specimen	B in.	W in.	b in.	P_m kip	P_m/B kip/in.	P_m/BW kip/in.^{2}	b/W	J_m kip/in.	S_y ksi	S_u ksi
I. Group A, K_{Ic} Data (K_{Ic} = 90.2 ksi$\sqrt{in.}$)[b]										
7	2.04	4.00	1.94	38.42	18.83	4.71	0.485	--	106	121
8			2.10	42.93	21.04	5.26	0.525	--		
9			1.92	37.39	18.33	4.58	0.480	--		
10			1.93	36.30	17.79	4.45	0.483	--		
II. Group B, J-Integral Data[c]										
5	1.00	2.00	0.67	6.58	6.58	3.28	0.335	0.251	106	121
3			0.49	4.02	4.02	2.00	0.245	0.268		
4			0.37	2.69	2.69	1.34	0.185	0.278		
2			0.33	2.25	2.25	1.12	0.165	0.270		
1			0.29	1.58	1.58	0.79	0.145	0.223		

a. Reference 14
b. Determined using ASTM E399 test method.
c. The average valid J_m value corresponds to K_{Ic} = 88 ksi$\sqrt{in.}$

TABLE 4
Test Results of 1EAFD Steel[a]
(Compact Specimen)

Specimen	B in.	W in.	b in.	P_m kip	P_m/B kip/in.	P_m/BW kip/in.^{2}	b/W	J_m kip/in.	S_y ksi	S_u ksi
I. Group A, K_{Ic} Data (K_{Ic} = 73.2)[b]										
2	1.02	2.00	0.95	11.63	11.40	5.70	0.475	--	161	171
4			0.90	9.79	9.60	4.80	0.450	--		
5			0.93	11.02	10.80	5.40	0.465	--		
6			0.94	11.54	11.31	5.66	0.470	--		
7			0.91	10.00	9.80	4.90	0.455	--		
II. Group B, J-Integral Data[c]										
2	0.50	2.00	0.68	3.16	1.58	3.16	0.340	0.292	161	171
3			0.45	1.52	0.76	1.52	0.225	0.231		
4			0.32	0.90	0.45	0.90	0.160	0.235		
5			0.25	0.58	0.29	0.58	0.125	0.178		
6			0.20	0.43	0.22	0.43	0.100	0.177		
7			0.16	0.27	0.14	0.27	0.080	0.175		

a. Reference 14
b. Determined using ASTM E399 test method.
c. The average valid J_m value corresponds to K_{Ic} = 80 ksi$\sqrt{in.}$

TABLE 5

Test Results of Ni-Cr-Mo-V Rotor Steel[a]
(Three-Point Bend Specimen)

Specimen	B in.	W in.	b in.	P_m kip	P_m/B kip/in.	P_m/BW kip/in.^{2}	b/W	J_m kip/in.	S_y ksi	S_u ksi
I. Series A, d = 1.58										
FC 1	0.394	0.474	0.351	5.70	14.47	30.53	0.741	0.950[b]	124	135
FC 2			0.355	5.92	15.03	31.71	0.749			
FC 3			0.306	4.47	11.35	23.95	0.646			
FC 4			0.301	4.32	10.96	23.12	0.635			
FC 5			0.260	3.36	8.53	18.00	0.549			
FC 6			0.256	3.27	8.30	17.51	0.540			
FC 7			0.209	2.27	5.76	12.15	0.441			
FC 8			0.213	2.41	6.12	12.91	0.449			
FC 9			0.125	0.86	2.18	4.60	0.264			
FC10			0.150	1.23	3.11	6.56	0.316			
FC12			0.118	0.73	1.84	3.88	0.249			
II. Series B, d = 3.90										
DFC3	0.788	0.948	0.586	11.90	15.10	15.93	0.618	1.02[c]	124	135
DFC6			0.496	8.10	10.28	10.84	0.523			
DFC8			0.305	3.10	3.93	4.15	0.322			
III. Series C, d = 3.70										
DFC1	0.788	0.948	0.478	8.52	10.81	11.40	0.504	1.02[c]	124	135
DFC2			0.340	4.34	5.51	5.81	0.359			

a. References 2 and 3
b. The average valid value of J_m corresponds to K_{Ic} = 177 ksi$\sqrt{\text{in.}}$
c. The average valid value of J_m corresponds to K_{Ic} = 183 ksi$\sqrt{\text{in.}}$

TABLE 6

Test Results of Low Strength AISI 4340 Steel[a]
(Four-Point Bend Specimen)

Specimen	B in.	W in.	b in.	P_m kip	P_m/B kip/in.	P_m/BW kip/in.^{2}	b/W	J_m[b] kip/in.	S_y ksi	S_u ksi
I. W = 1.00 in.										
A 1	0.25	1.00	0.135	0.21	0.83	0.83	0.135	0.63	113	127
A 2	0.25		0.452	1.88	7.52	7.52	0.452	1.35		
A 5	0.50		0.219	1.03	2.06	2.06	0.219	0.83		
A 6	0.50		0.187	0.79	1.58	1.58	0.187	0.77		
A 7	0.50		0.330	2.22	4.44	4.44	0.330	1.06		
A 8	0.50		0.444	3.81	7.62	7.62	0.444	0.87		
A10	0.75		0.213	1.48	1.97	1.97	0.213	0.95		
A11	0.75		0.298	2.79	3.72	3.72	0.298	0.94		
A12	0.75		0.454	6.86	9.15	9.15	0.454	0.95		
A16	1.00		0.282	3.54	3.54	3.54	0.282	0.96		
A17	1.00		0.393	6.30	6.50	6.50	0.393	0.97		
A20	1.50		0.185	2.55	1.70	1.70	0.185	0.92		
A21	1.50		0.432	11.76	7.84	7.84	0.432	0.95		
A25	2.00		0.198	3.74	1.87	1.87	0.198	0.91		
A26	2.00		0.378	12.47	6.24	6.24	0.378	0.98		
II. W ≠ 1.00										
A50	0.118	1.000	0.164	0.125	1.06	1.06	0.164	1.14	113	127
A51	0.126	0.826	0.054	0.016	0.13	0.15	0.065	0.51		
A52	0.126	0.807	0.052	0.016	0.12	0.16	0.064	0.45		
A53	0.126	0.834	0.082	0.039	0.31	0.37	0.098	0.60		
A54	0.187	0.847	0.077	0.050	0.27	0.32	0.091	0.65		
A55	0.186	0.845	0.079	0.051	0.28	0.32	0.093	0.53		
A56	0.187	0.862	0.079	0.052	0.28	0.32	0.092	0.69		
A57	0.186	0.844	0.115	0.103	0.55	0.66	0.136	0.90		
A58	0.250	0.844	0.113	0.143	0.57	0.68	0.134	0.75		
A59	0.249	0.844	0.115	0.145	0.58	0.69	0.136	0.72		

a. Reference 21
b. The average valid J_m value corresponds to K_{Ic} = 178 ksi$\sqrt{\text{in.}}$

TABLE 7

Test Results of A514F Steel[a]
(Four-Point Bend Specimen)

Specimen	B in.	W in.	b in.	P_m kip	P_m/B kip/in.	P_m/BW kip/in.^{2}	b/W	J_m kip/in.	S_y ksi	S_u ksi
I. Orientation A (LT)[b]										
A 5	0.188	0.719	0.36	0.840	4.47	6.22	0.50	0.41	110	117
A10	0.123		0.14	0.095	0.77	1.07	0.19	0.77		
A12	0.248		0.24	0.518	2.09	2.91	0.33	1.20		
A13	0.375		0.36	1.672	4.46	6.20	0.50	0.46		
A14	0.199		0.19	0.294	1.48	2.06	0.26	0.50		
A15	0.299		0.28	0.847	2.83	3.94	0.39	0.41		
A20	0.249		0.13	0.164	0.66	0.92	0.18	0.71		
A21	0.400		0.18	0.554	1.39	1.93	0.25	0.68		
A22	0.501		0.24	1.123	2.24	3.12	0.33	1.66		
A24	0.750		0.36	3.650	4.87	6.77	0.50	0.37		
A30	0.188		0.13	0.126	0.67	0.93	0.18	0.41		
A31	0.250		0.14	0.227	0.91	1.27	0.19	0.67		
A32	0.372		0.22	0.770	2.07	2.88	0.31	0.53		
A40	0.499		0.19	0.722	1.45	2.02	0.26	0.53		
A41	0.750		0.26	2.135	2.85	3.96	0.36	0.47		

TABLE 7 (Cont'd.)

Specimen	B in.	W in.	b in.	P_m kip	P_m/B kip/in.	P_m/BW kip/in.^{2}	b/W	J_m kip/in.	S_y ksi	S_u ksi
II. Orientation B (TL)[c]										
B 1	0.720	0.750	0.11	0.332	0.46	0.61	0.15	0.31	110	117
B 2	0.500		0.13	0.313	0.63	0.84	0.17	0.34		
B 3	0.300		0.13	0.180	0.60	0.80	0.17	0.28		
B 4	0.198		0.13	0.111	0.56	0.75	0.17	0.27		
B10	0.720		0.19	1.087	1.51	2.01	0.25	0.34		
B11	0.500		0.18	0.620	1.24	1.65	0.24	0.30		
B12	0.300		0.21	0.525	1.75	2.33	0.28	0.35		
B13	0.198		0.19	0.244	1.23	1.64	0.25	0.33		
B20	0.720		0.29	2.304	3.20	4.27	0.39	0.32		
B21	0.499		0.28	1.487	2.98	3.97	0.37	0.34		
B22	0.300		0.30	0.960	3.20	4.27	0.40	0.21		
B23	0.198		0.30	0.622	3.14	4.19	0.40	0.52		
B30	0.720		0.31	2.490	3.46	4.61	0.41	0.30		
B31[d]	0.499		0.35	2.240	4.49	5.99	0.49	0.31		
B32	0.300		0.33	1.195	3.98	5.31	0.44	0.45		
B33	0.198		0.35	0.813	4.11	5.48	0.47	1.01		

a. Reference 22
b. The average valid value of J_m corresponds to K_{Ic} = 133 ksi$\sqrt{in.}$
c. The average valid value of J_m corresponds to K_{Ic} = 104 ksi$\sqrt{in.}$
d. W = 0.713 in.

TABLE 8

Test Results of High Strength AISI 4340 Steel[a]
(Four-Point Bend Specimen)

Specimen	B in.	W in.	b in.	P_m kip	P_m/B kip/in.	P_m/BW kip/in.^{2}	b/W	J_m[b] kip/in.	S_y ksi	S_u ksi
I. W = 1.00 in.										
B 0	0.25	1.00	0.233	0.69	2.76	2.76	0.233	0.45	174	189
B 1	0.25		0.348	1.39	5.56	5.56	0.348	0.55		
B 2	0.25		0.489	2.49	9.96	9.96	0.489	0.59		
B 5	0.50		0.217	1.29	2.58	2.58	0.217	0.46		
B 6	0.50		0.178	0.96	1.92	1.92	0.178	0.47		
B 7	0.50		0.314	2.37	4.74	4.74	0.314	0.59		
B 8	0.50		0.451	4.55	9.10	9.10	0.451	0.59		
B10	0.75		0.202	1.70	2.27	2.27	0.202	0.47		
B12	0.75		0.416	5.87	7.83	7.83	0.416	0.50		
B15	1.00		0.196	2.25	2.25	2.25	0.196	0.46		
B16	1.00		0.304	4.62	4.62	4.62	0.304	0.48		
B17	1.00		0.422	7.87	7.87	7.87	0.422	0.46		
B21	1.50		0.446	13.20	8.80	8.80	0.446	0.49		
B25	2.00		0.222	5.07	2.54	2.54	0.222	0.46		
B26	2.00		0.301	9.17	4.59	4.59	0.301	0.48		
B27	2.00		0.381	13.57	6.79	6.79	0.381	0.49		
II. W ≠ 1.00 in.										
B50	0.122	0.859	0.055	0.023	0.19	0.22	0.064	0.20	174	189
B51	0.125	0.837	0.051	0.020	0.16	0.19	0.061	0.19		
B52	0.120	0.836	0.053	0.020	0.17	0.20	0.063	0.20		
B53	0.192	0.851	0.080	0.077	0.40	0.47	0.094	0.31		
B54	0.189	0.863	0.080	0.072	0.38	0.44	0.093	0.29		
B55	0.250	0.841	0.106	0.158	0.63	0.75	0.126	0.33		

a. Reference 21
b. The average valid value of J_m corresponds to K_{Ic} = 125 ksi$\sqrt{\text{in.}}$

Table 9

Chemical Compositions of Base Metal and Welding Electrode*

	Base Metal**	Welding Electrode
Designation:	A514 Grade F	GMAW 110 ksi yield
Material Dimensions:	3/4 in. plate	1/16 in. bare wire
Element	Chemical Composition in Weight Percent	
C	0.16	0.08
Mn	0.82	1.70
P	0.012	0.005
S	0.019	0.009
Si	0.23	0.46
Cu	0.27	--
Ni	0.76	2.40
Cr	0.54	0.05
Mo	0.47	0.50
V	0.06	0.02
B	0.004	--
Al	--	0.003
Ti	--	0.025

* Compositions supplied by manufacturer

** Ladle composition

TABLE 10

Test Results of Specimens Containing Full-Length IJP Discontinuities Welded with Different Heat Inputs

Specimen	2a in.	S_y[a] ksi	S_m ksi	e_m in./in.	e_f in./in.	R.A. %	J_n kip/in.
6125[be]	0.177	83.1	84.9	0.007	0.017	6.85	0.53
6130[b]	0.160	102.4	106.6	0.010	0.014	5.05	1.02
6135[b]	0.224	75.5	90.4	0.014	0.018	5.95	1.33
6225[c]	0.199	109.0	113.0	0.012	0.014	4.24	1.29
6230[c]	0.240	97.8	115.9	0.009	0.011	2.71	1.12
6235[c]	0.254	98.8	102.6	0.008	0.014	4.76	1.19
6325[d]	0.112	89.9	106.1	0.013	0.022	6.76	1.05
6330[d]	0.238	62.0	74.9	0.017	0.034	8.75	1.08
6335[d]	0.222	71.8	81.6	0.015	0.026	9.79	1.31

a. 0.20 percent offset yield strength.
b. 50 kJ/in. heat input.
c. 20 kJ/in. heat input.
d. 90 kJ/in. heat input.
e. Contained secondary defects.

TABLE 11

Test Results of Specimens Containing As-Welded, Full-Length IJP Discontinuities
(30 kJ/in. Heat Input)

Specimen	2a in.	S_y[a] ksi	S_m ksi	S_n ksi	e_m in./in.	e_f in./in.	R.A. %	J_m kip/in.
1205[b]	---	113	128	---	0.088	---	32.2	---
1210[b]	~0.03	108	122	---	0.092	---	38.2	---
1215[b]	0.065	112	123	137	0.048	0.049	3.35	11.10
1220[b]	0.124	104	112	135	0.012	0.013	3.69	2.05
1225[b]	0.156	105	117	151	0.043	0.044	6.91	11.16
1230	0.216	77	107	149	0.015	0.023	4.52	1.70[c]
1235	0.242	77	99	151	0.012	0.019	4.31	1.34[c]
1240	0.274	68	98	161	0.011	0.012	4.32	1.33[c]
1315	~0.03	108	128	---	---	---	---	---
1320	0.119	108	118	142	0.021	0.041	7.50	2.36
1325	0.102	103	120	142	0.061	0.062	7.92	7.50
1330	0.180	96	107	145	0.014	0.021	5.73	1.59[c]
1335	0.199	100	109	152	0.012	0.013	3.55	1.30[c]
1340	0.232	103	113	170	0.010	0.011	4.14	1.07[c]
1345	0.231	99	112	168	0.014	0.015	3.66	1.69[c]
							Avg. J_m	= 1.43

a. 0.20 percent offset yield strength.
b. 2.00 in. gage length used in these tests only. 1.00 in. gage length used all other tests.
c. Valid J_m, 2a > .135 in.

TABLE 12

Test Results of Specimens Containing Inclined Full-Length IJP Discontinuities
(30 kJ/in. Heat Input)

Specimen	2a[a] in.	IJP Angle deg	S_y[b] ksi	S_m ksi	S_n ksi	e_m in./in.	e_f in./in.	R.A. %	J_m kip/in.
3130	0.175	10	117	121	161	0.016	0.018	3.76	1.91[c]
3230	0.184	20	108	109	148	0.008	0.015	4.78	0.79[c]
3330	0.128	30	114	126	154	0.066	0.077	4.45	8.60
3430	0.105	40	118	127	150	0.035	0.037	6.86	4.27
3530	0.133	50	110	113	140	0.008	0.010	5.60	0.95[c]

a. Projected length of IJP on plane normal to the applied load.
b. 0.20 percent offset yield strength.
c. Valid J_m, $2a > 0.135$ in.

TABLE 13

Test Results of Specimens Containing Fatigue Sharpened, Full-Length IJP Discontinuities
(30 kJ/in. Heat Input)

Specimen	$2a_o$ in.	Fatigued 2a in.	ΔK ksi$\sqrt{in.}$	S_y[a] ksi	S_m ksi	S_n ksi	e_m in./in.	e_f in./in.	R.A. %	J_m kip/in.
4120[b]	0.101	0.188	9.34	100	110	154	0.020	0.050	4.75	2.50[e]
4125[b]	0.175	0.269	12.83	87	100	159	0.017	0.027	6.78	2.09[e]
4130[b]	0.170	0.182	10.28	96	108	149	0.011	0.036	6.60	1.05[e]
4220[c]	0.094	0.217	20.10	86	98	148	0.014	0.019	4.98	1.44[e]
4225[c]	0.108	0.132	22.10	109	121	161	0.057	0.059	5.57	7.02
4230[cd]	0.218	0.551	33.70	--	--	--	--	--	--	--

a. 0.20 percent offset yield strength.
b. Fatigue precracked at about 20 percent net section yield strength.
c. Fatigue precracked at about 50 percent net section yield strength.
d. Failed in fatigue.
e. Valid J_m, 2a > 0.135 in.

TABLE 14

Test Results of Specimens Welded with Various V-Groove Preparation Angles Containing Full-Length IJP Discontinuities (30 kJ/in. Heat Input)

Specimen	2a in.	Groove Angle, deg.	S_y[a] ksi	S_m ksi	S_n ksi	e_m in./in.	e_f in./in.	R.A. %	J_m kip/in.
7125	0.041	90	115	123	134	0.080	0.090	7.99	9.41
7225	0.178	40	106	106	146	0.010	0.016	3.74	1.06[b]

a. 0.20 percent offset yield strength.
b. Valid J_m, 2a > 0.135 in.

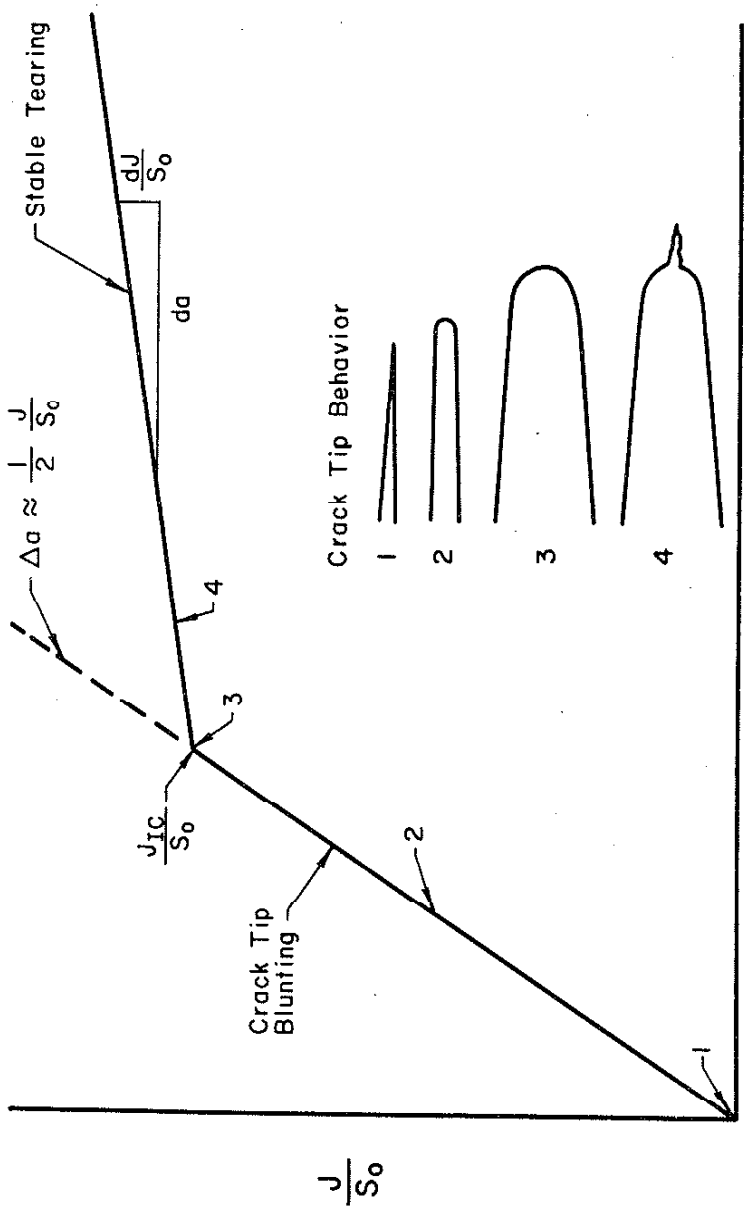

Fig. 1 J-integral R-curve illustrating the crack tip behavior as J increases. The crack tip blunts in the region $0 < J/S_o < J_{Ic}/S_o$ followed by stable crack extension by tearing when $J/S_o > J_{Ic}/S_o$.

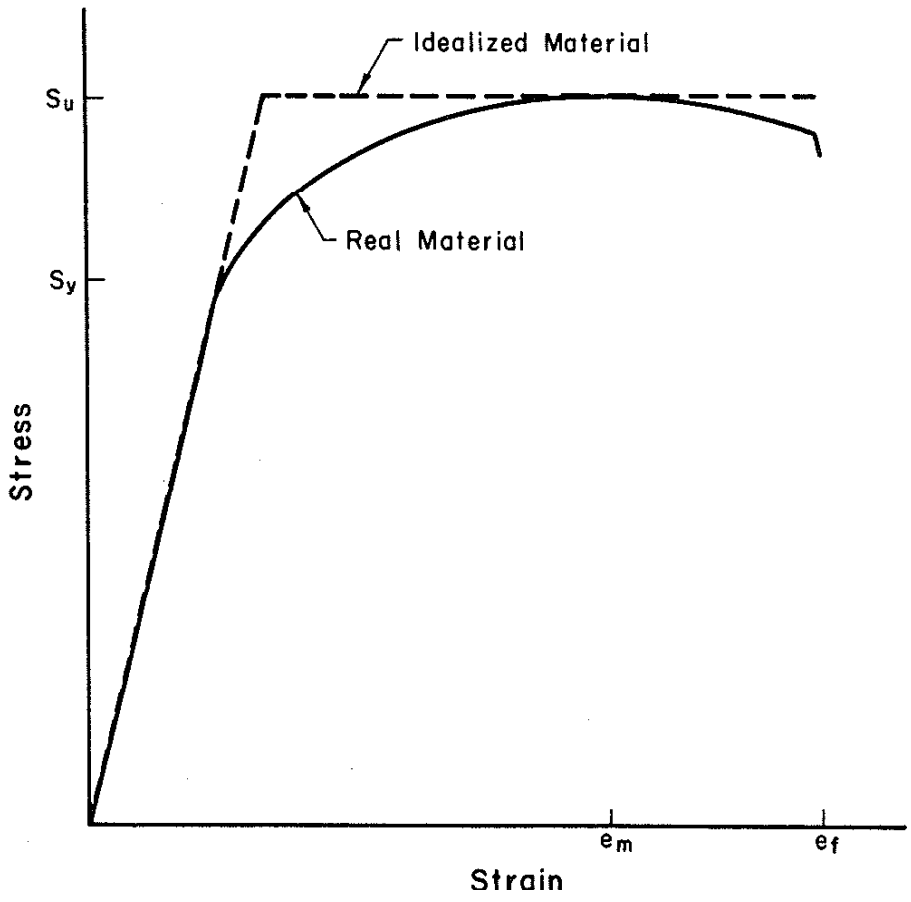

Fig. 2 Stress-strain curves for a real material and its idealization; both curves have the same tensile strength, S_u.

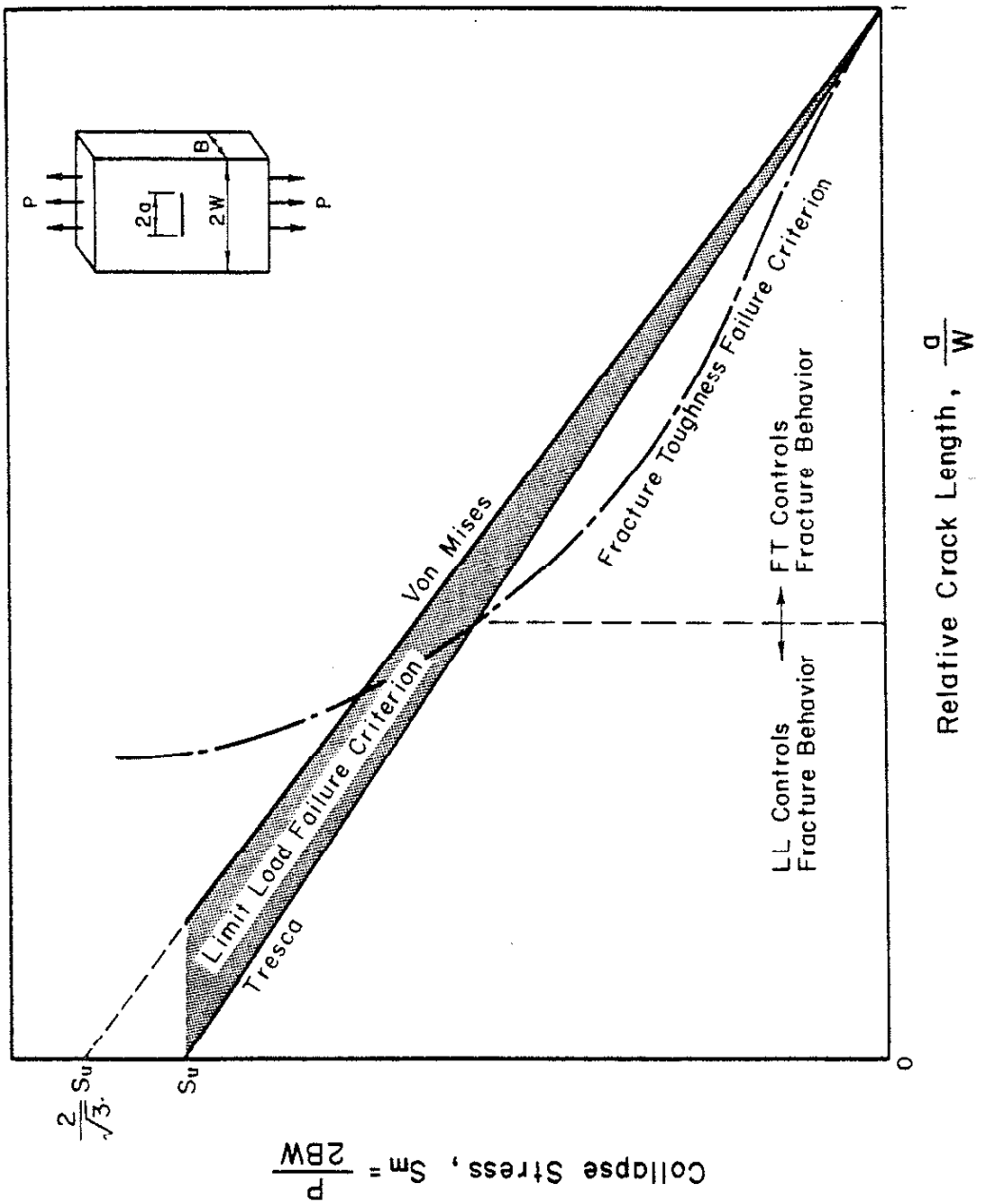

Fig. 3 Illustration of the two failure criteria model for a center-crack tension specimen.

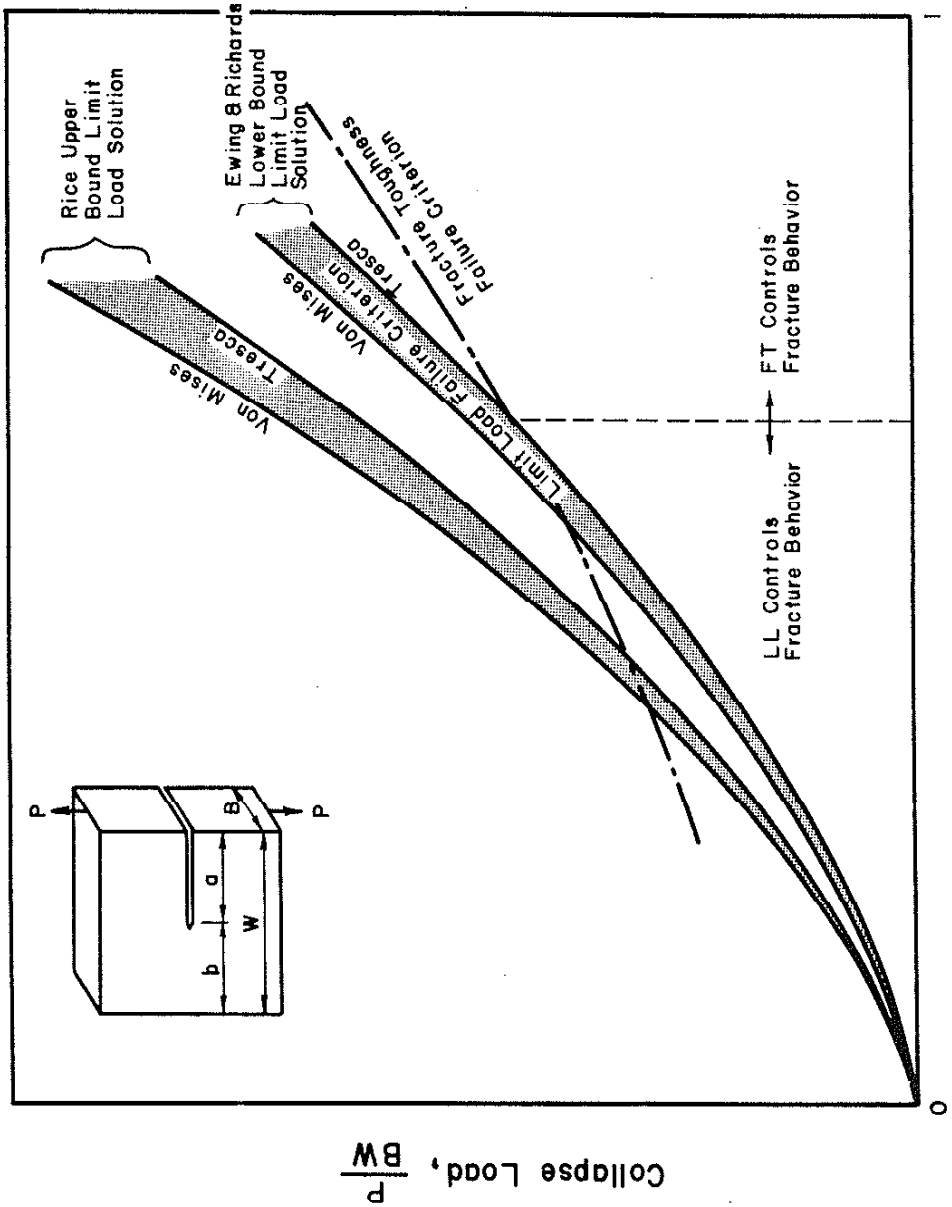

Fig. 4 Illustration of the two failure criteria model for the compact specimen whose limit load failure criterion is approximated by upper and lower bound limit load solutions.

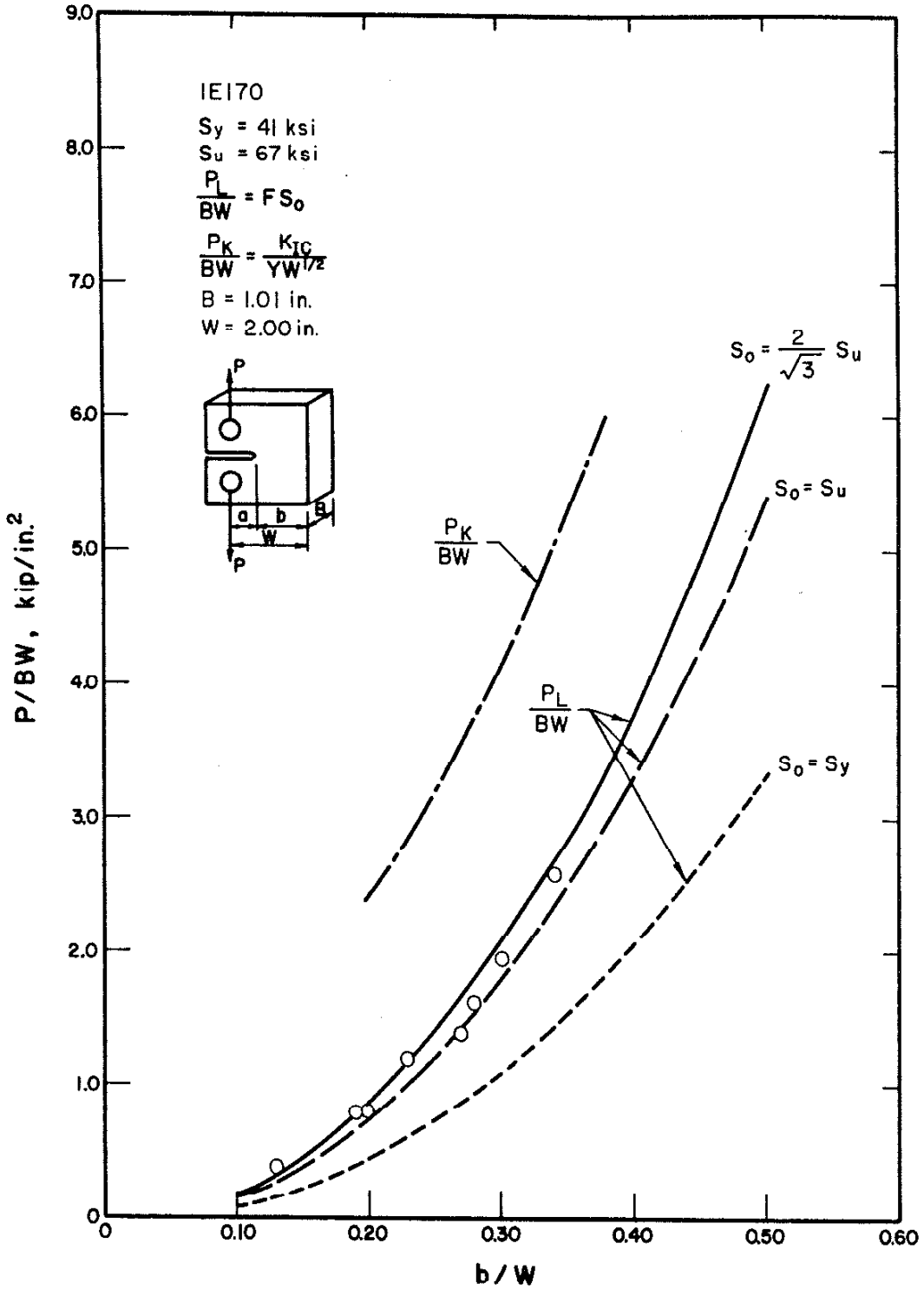

Fig. 5 Comparison of 1E170 steel compact specimen data with collapse loads predicted by the limit load and fracture toughness failure criteria [14].

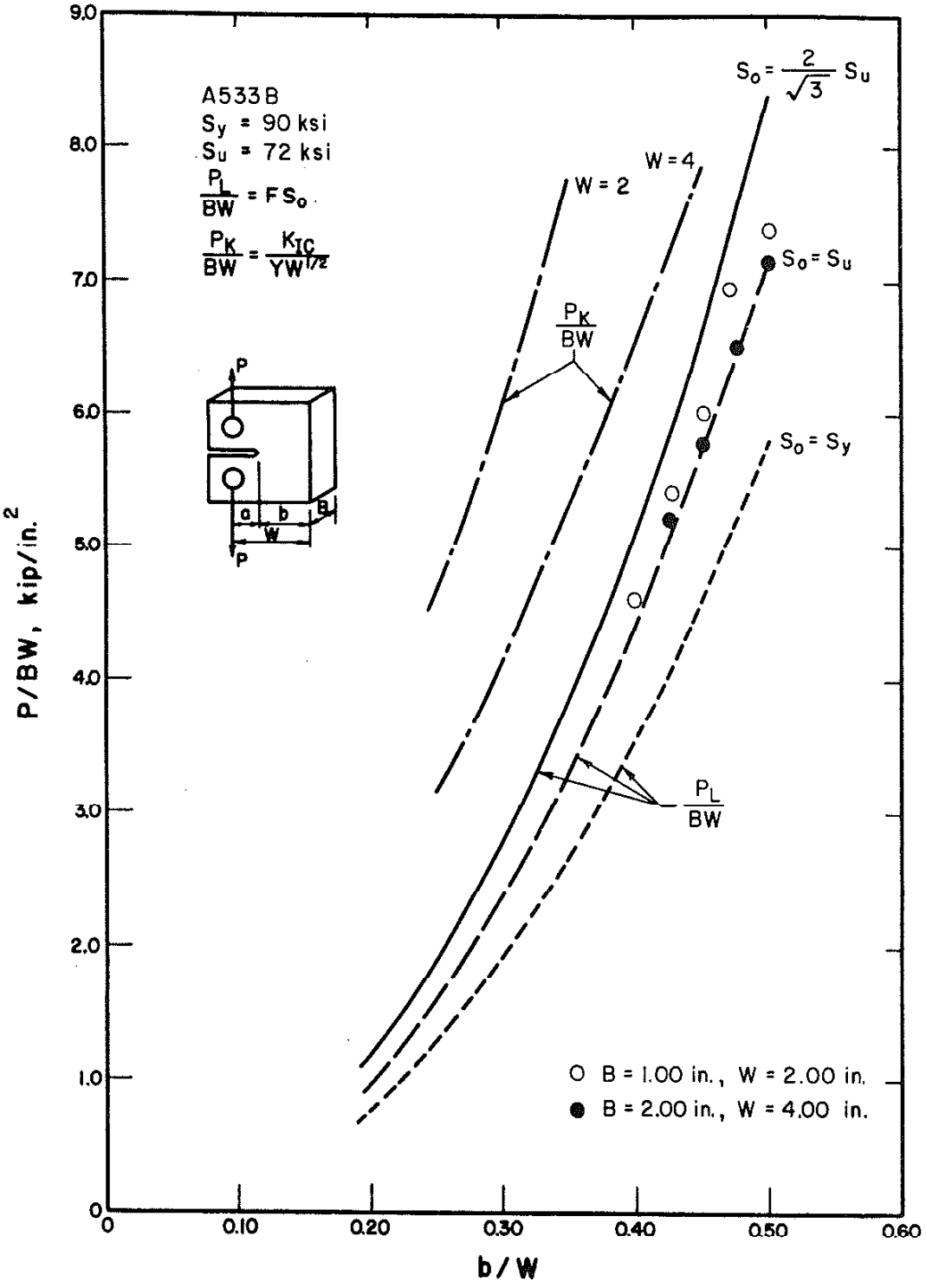

Fig. 6 Comparison of A533B steel compact specimen data with collapse loads predicted by the limit load and fracture toughness failure criteria [2, 3].

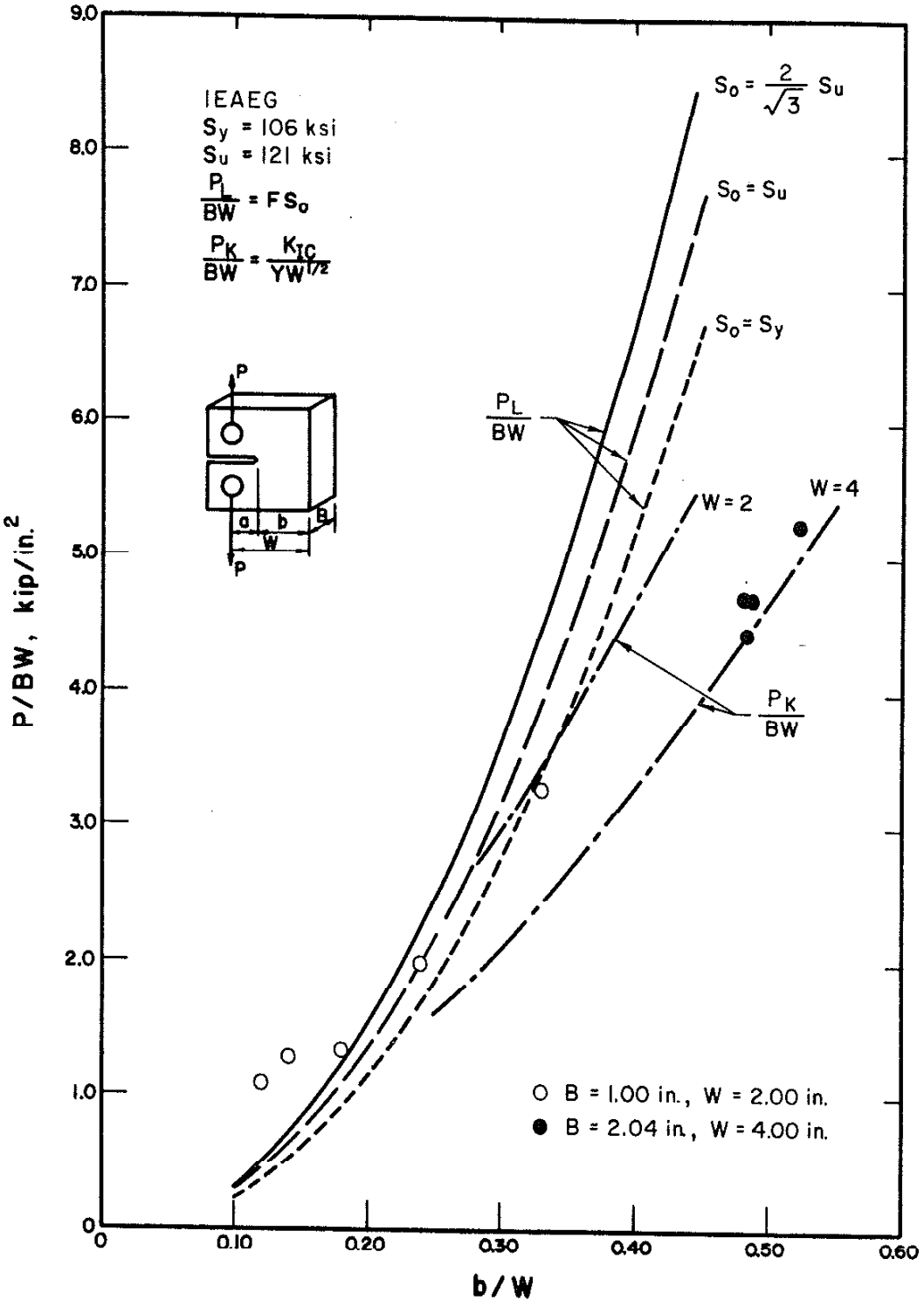

Fig. 7 Comparison of IEAEG steel compact specimen data with collapse loads predicted by the limit load and fracture toughness failure criteria [14].

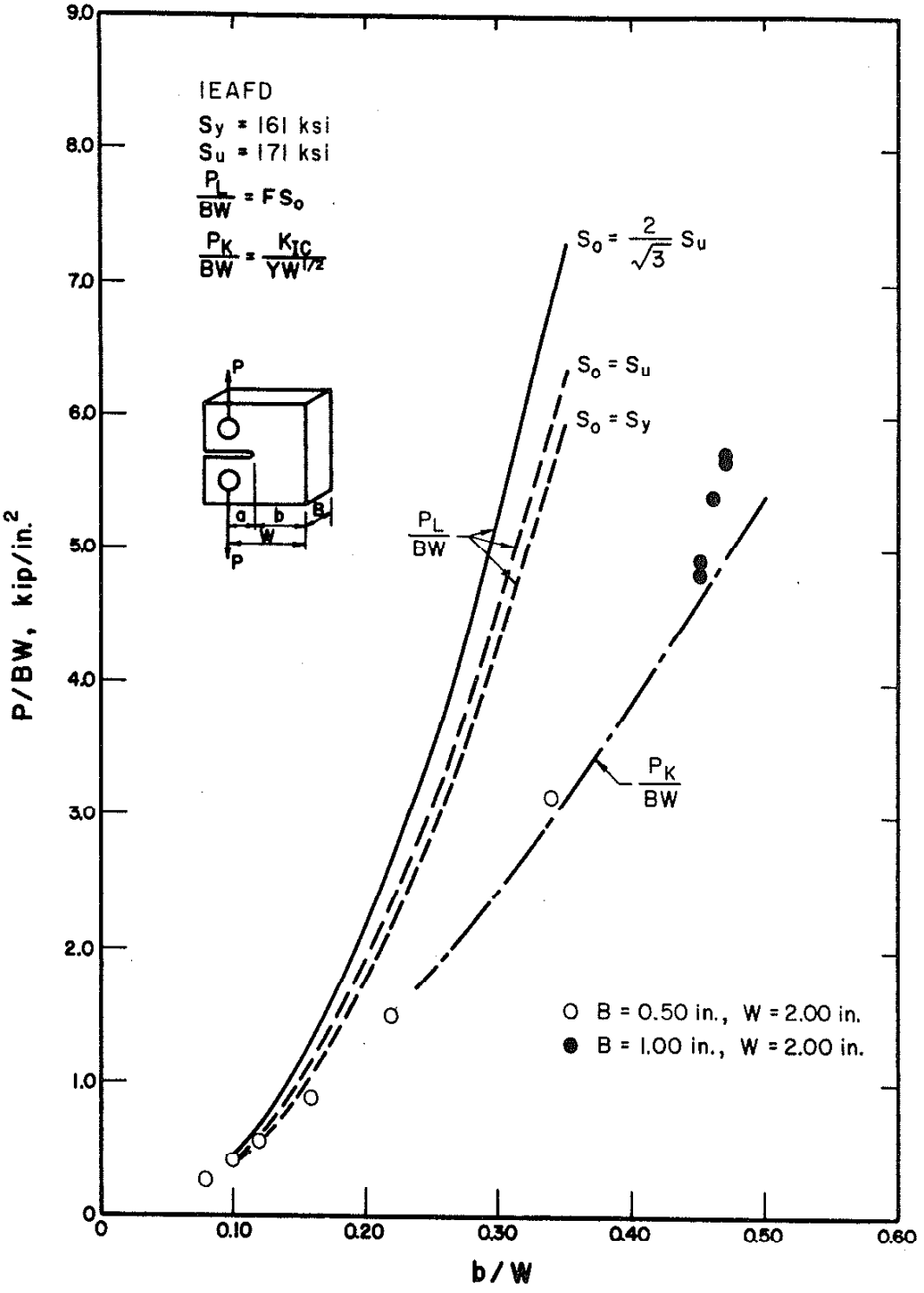

Fig. 8 Comparison of 1EAFD steel compact specimen data with collapse loads predicted by the limit load and fracture toughness failure criteria [14].

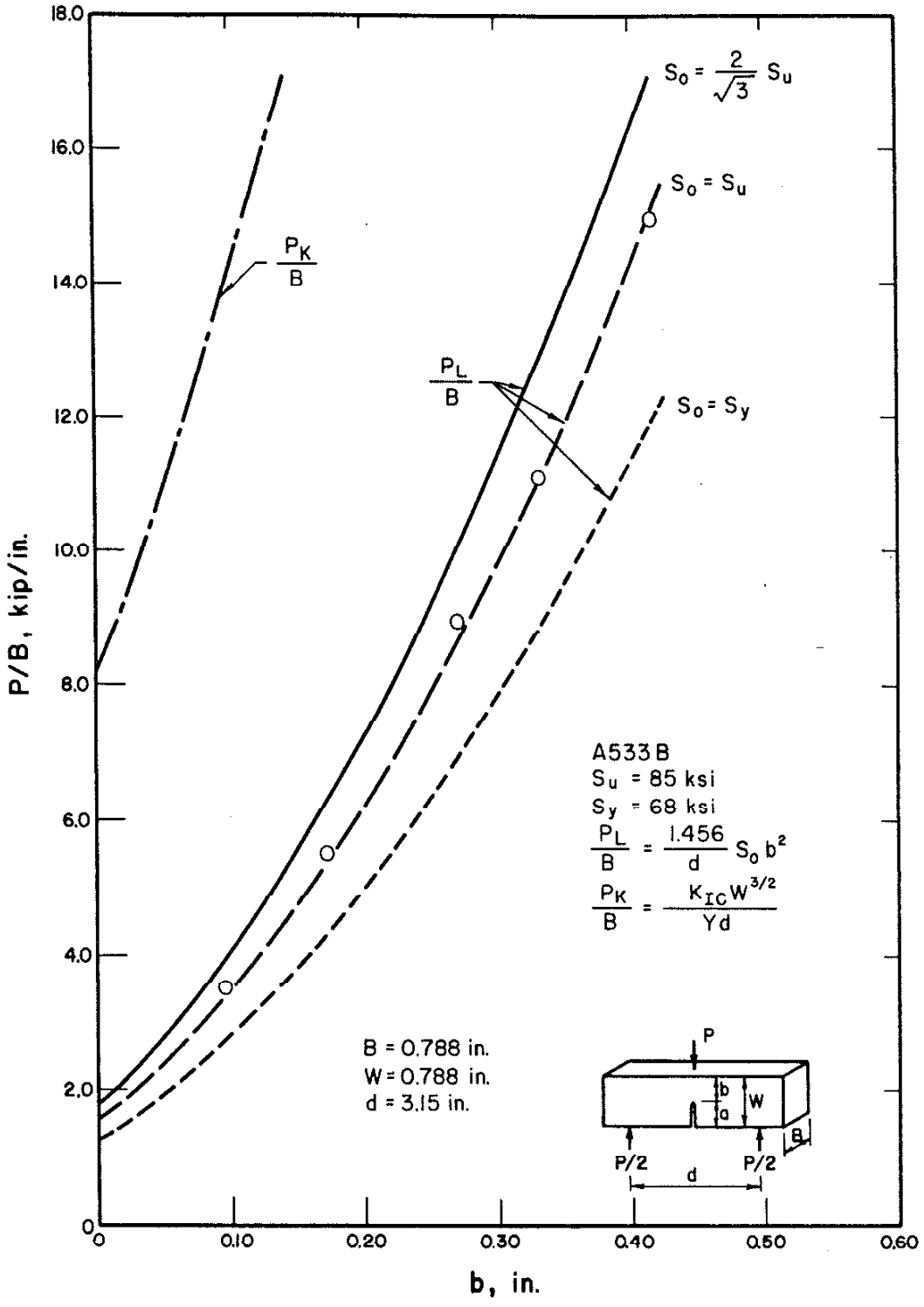

Fig. 9 Comparison of A533B steel three-point bend specimen data with collapse loads predicted by the limit load and fracture toughness failure criteria [2, 3].

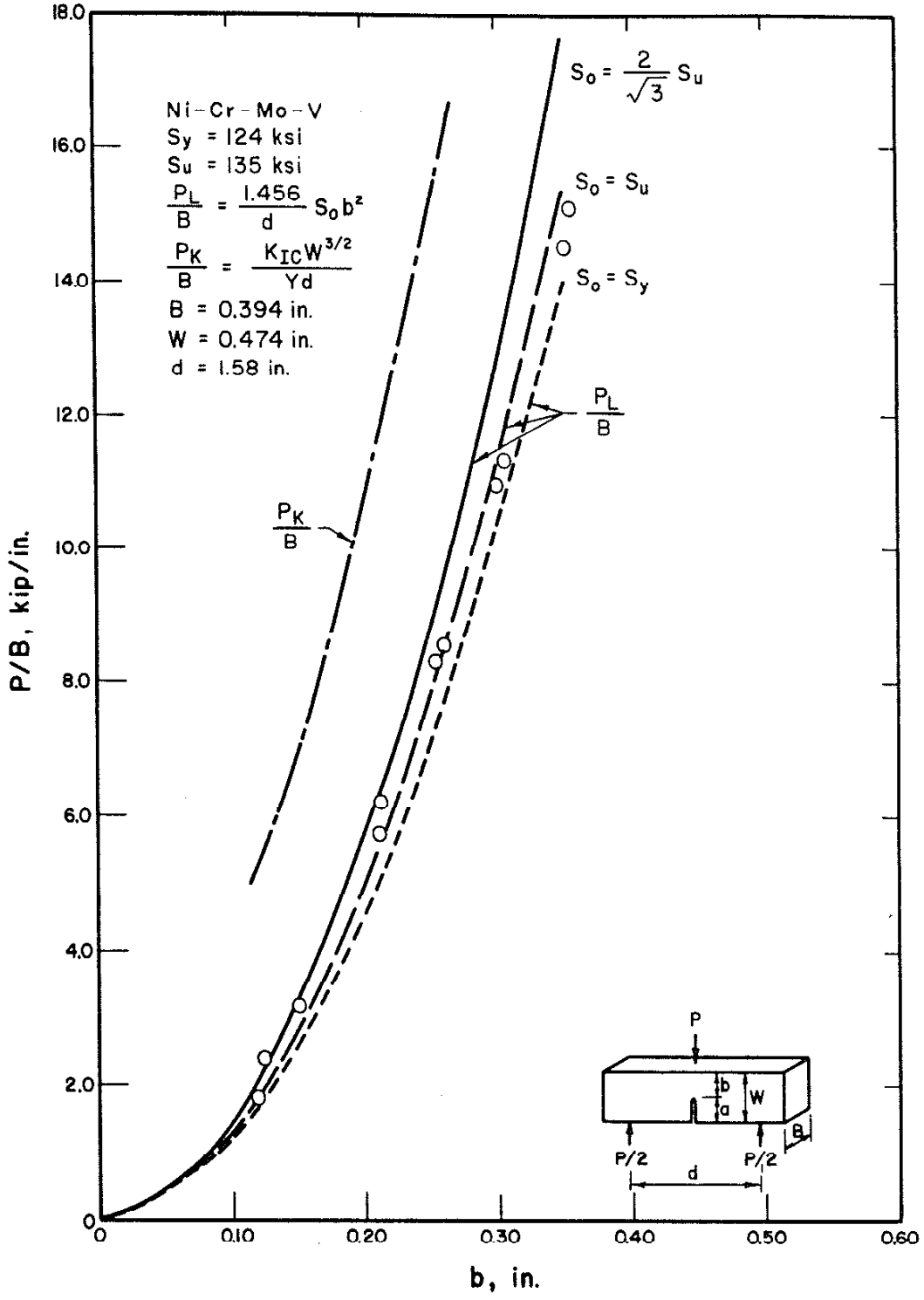

Fig. 10 Comparison of Ni-Cr-Mo-V steel three-point bend specimen data with collapse loads predicted by the limit load and fracture toughness failure criteria [2, 3].

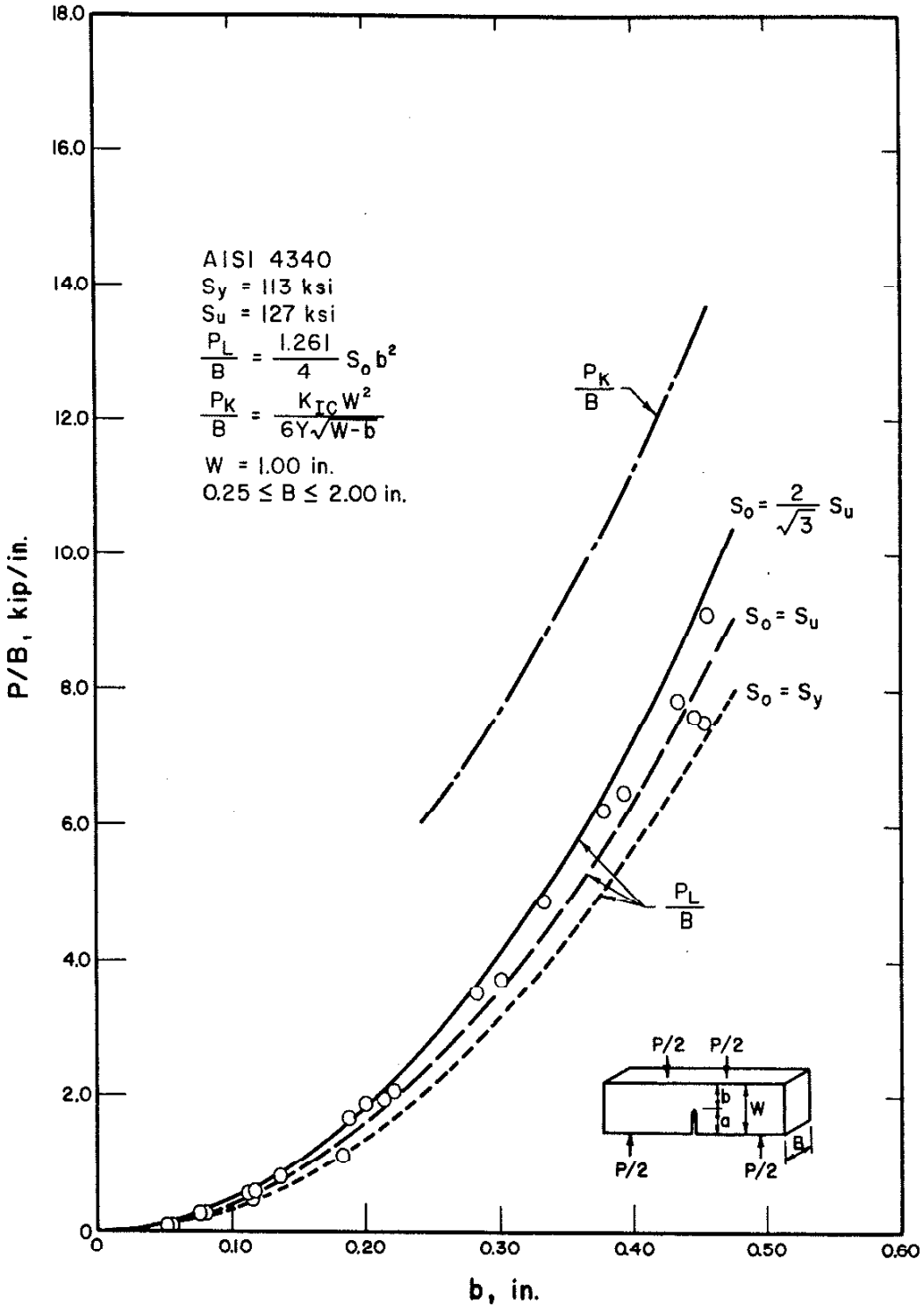

Fig. 11 Comparison of low-strength AISI 4340 steel four-point bend specimen data with collapse loads predicted by the limit load and fracture toughness failure criteria [21].

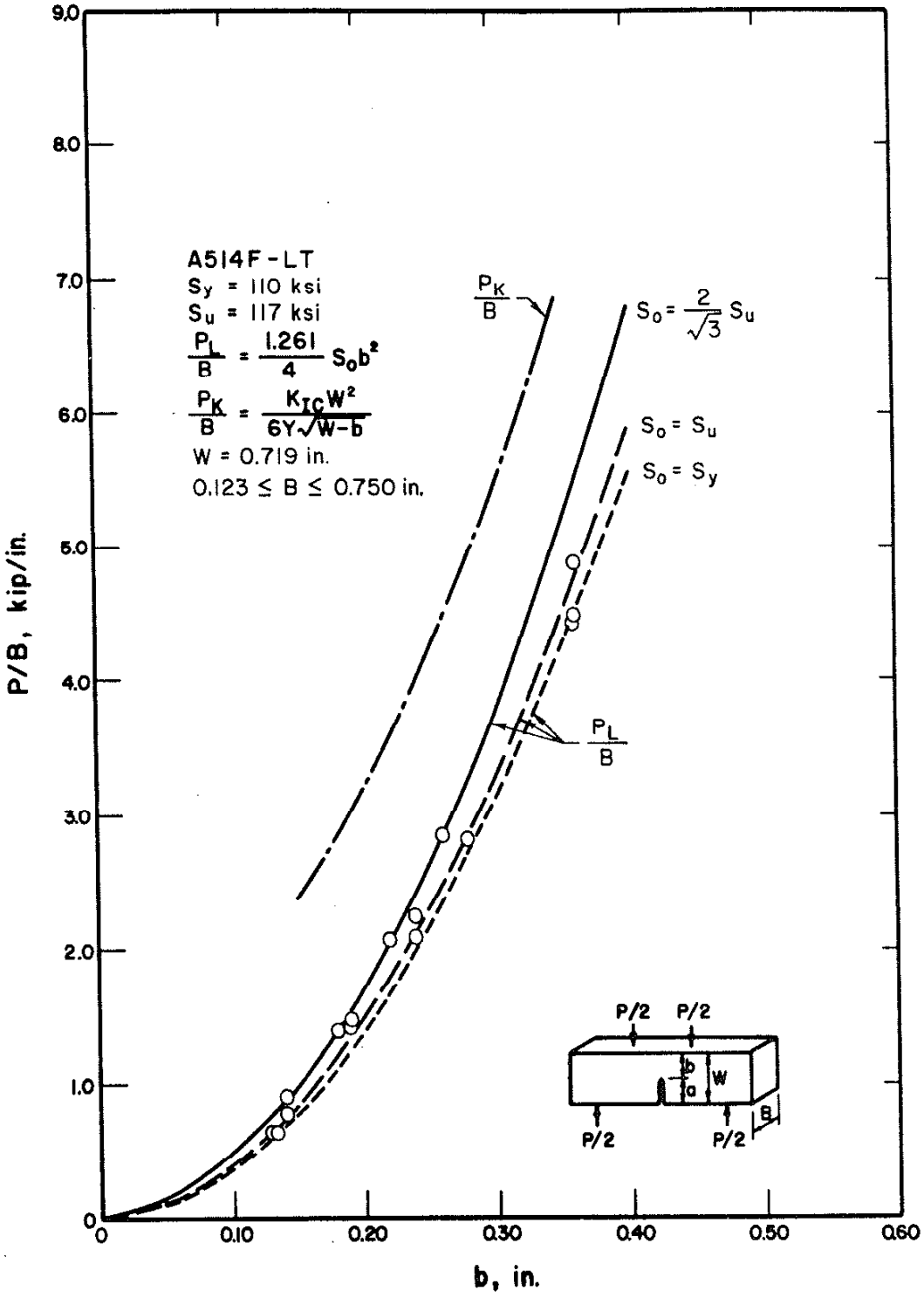

Fig. 12 Comparison of A514F-LT steel four-point bend specimen data with collapse loads predicted by the limit load and fracture toughness failure criteria [22].

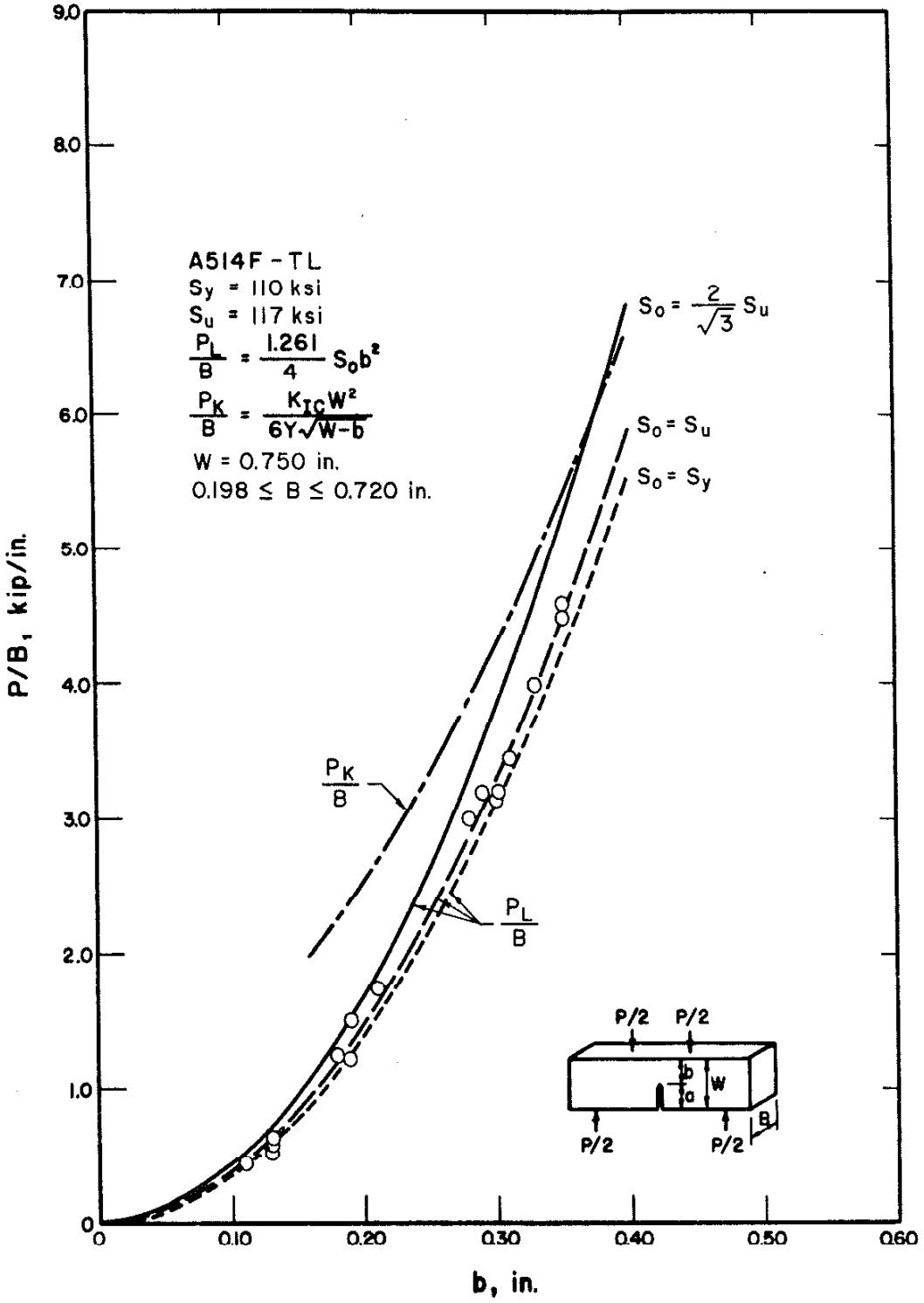

Fig. 13 Comparison of A514F-TL steel four-point bend specimen data with collapse loads predicted by the limit load and fracture toughness failure criteria [22].

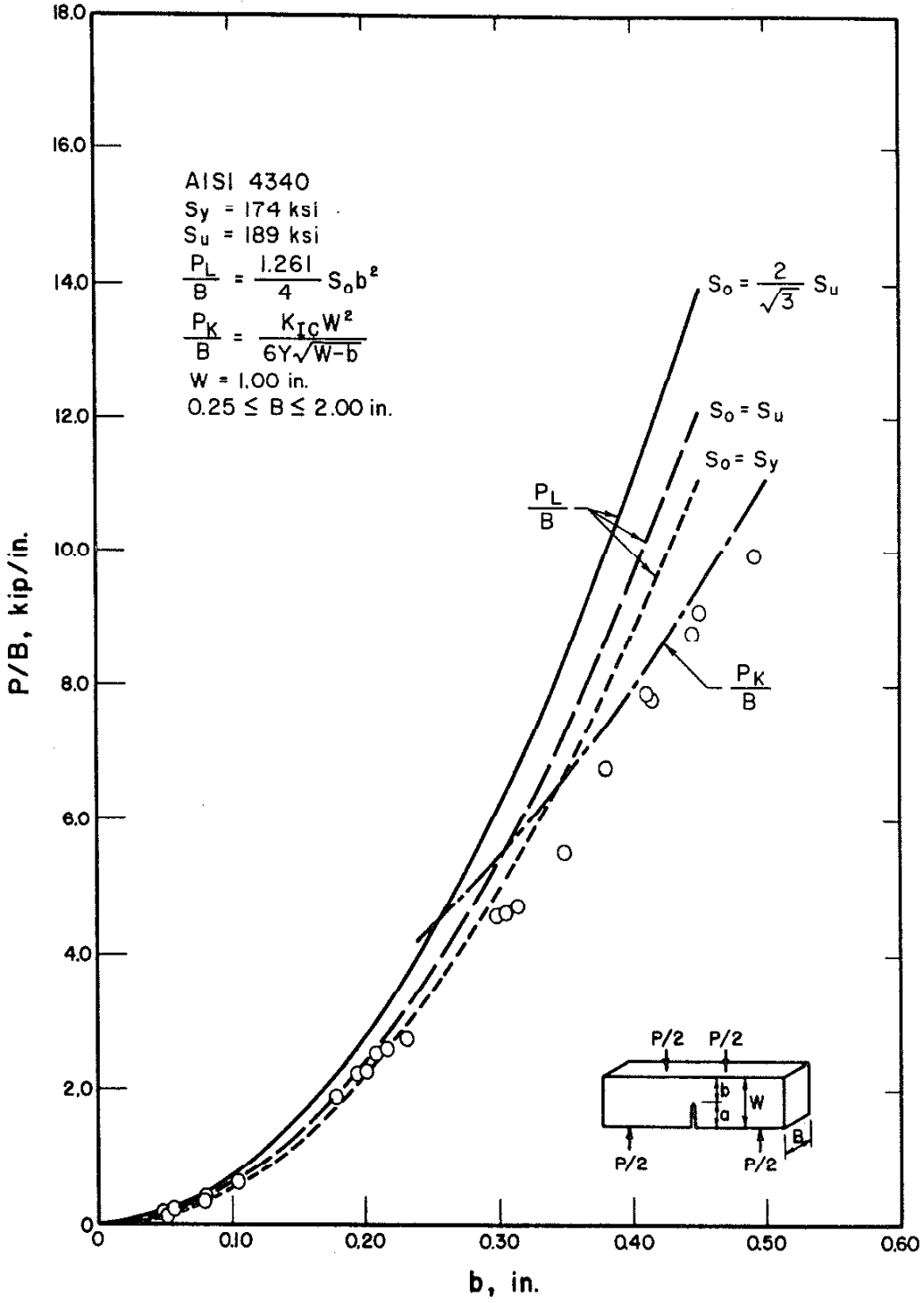

Fig. 14 Comparison of high-strength AISI 4340 steel four-point bend specimen data with collapse loads predicted by the limit load and fracture toughness failure criteria [21].

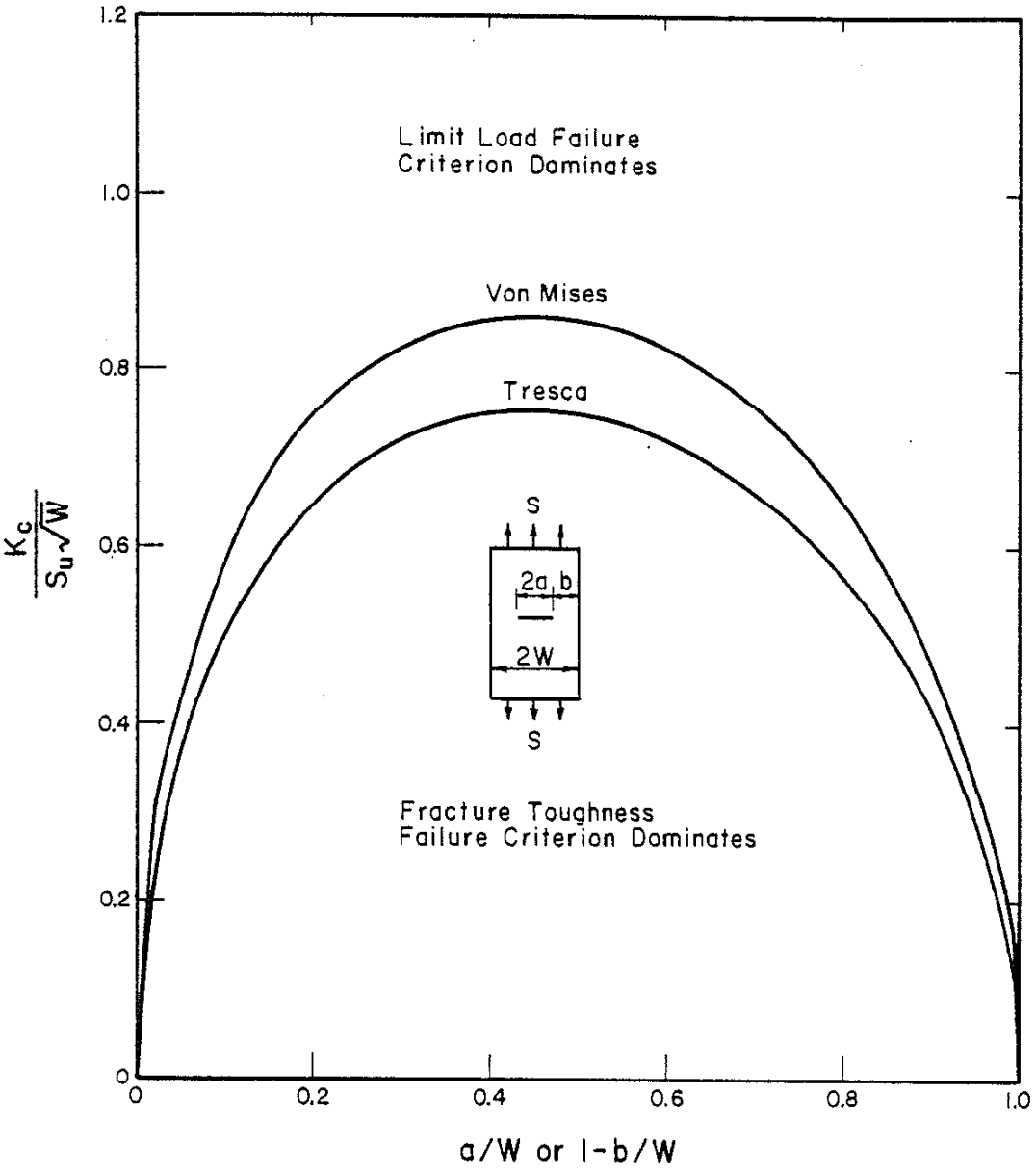

Fig. 15 Limit load and fracture toughness failure criteria controlled fracture regions for the center-crack tension specimen.

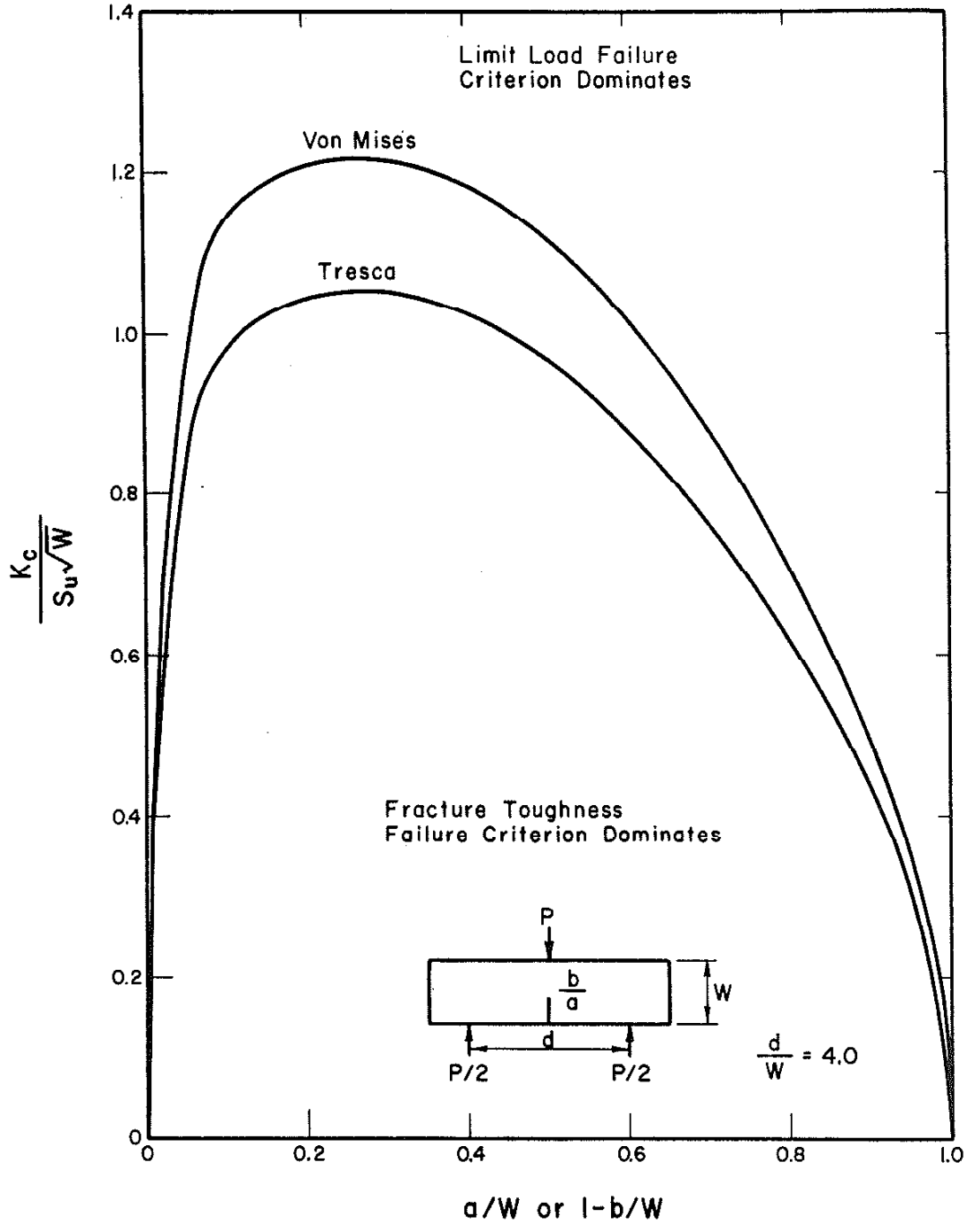

Fig. 16 Limit load and fracture toughness failure criteria controlled fracture regions for the three-point bend specimen.

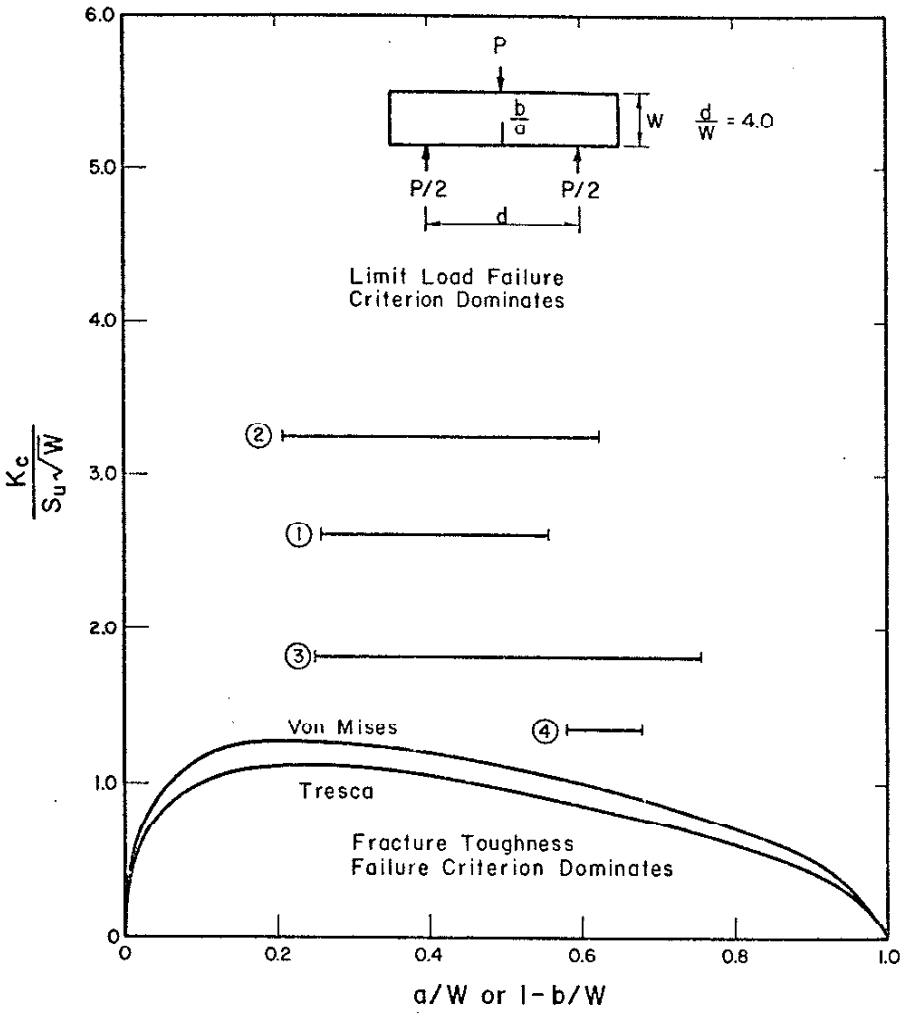

① Ni-Cr-Mo-V	W = 0.474	B = 0.788	S_u = 135
② A533 B	0.788	0.788	90
③ Ni-Cr-Mo-V	0.474	0.394	135
④ Ni-Cr-Mo-V	0.948	0.788	135

Fig. 17 Comparison of three-point bend specimen data from a variety of steels with the controlling failure criterion prediction shown in Fig. 16. All the data shown were limit load failures.

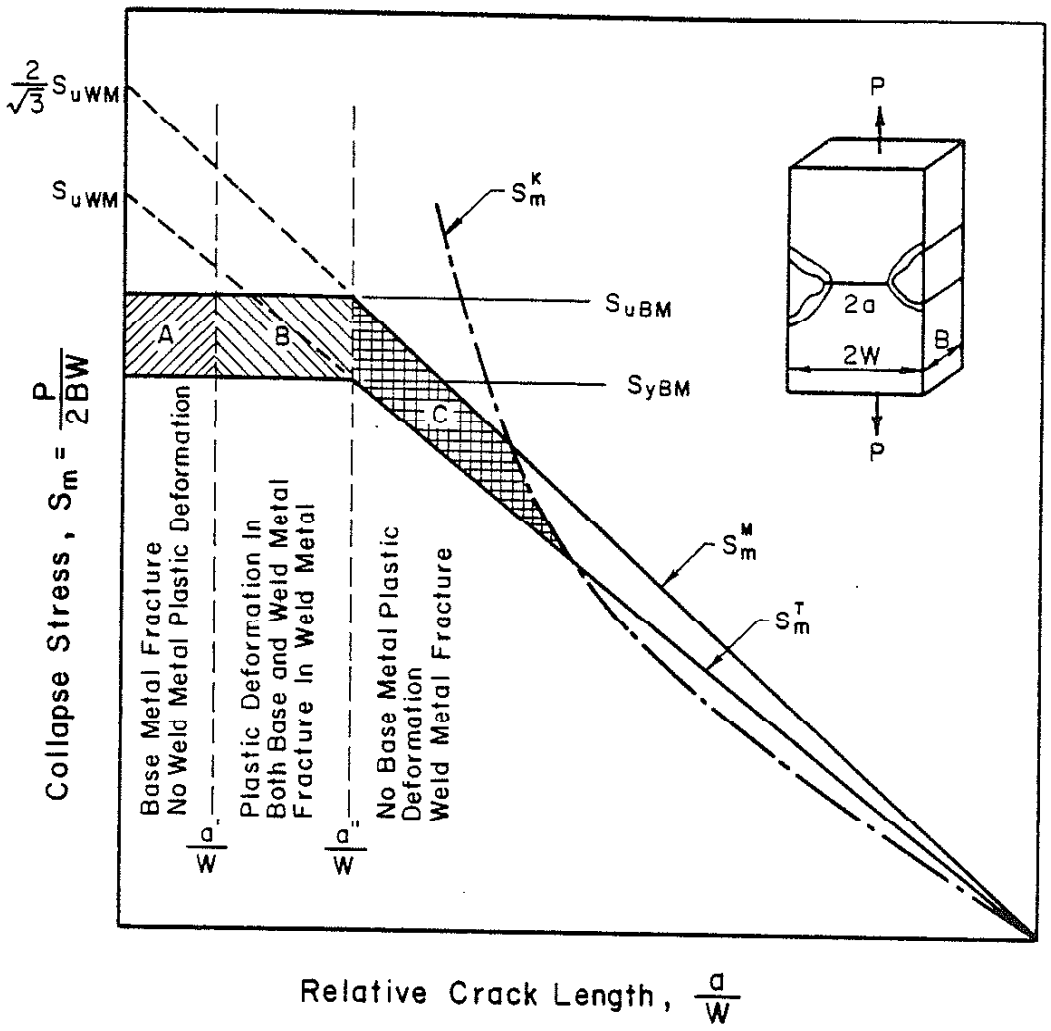

Fig. 18 Extension of the two failure criteria model to overmatched, high fracture toughness, butt weldments containing planar discontinuities.

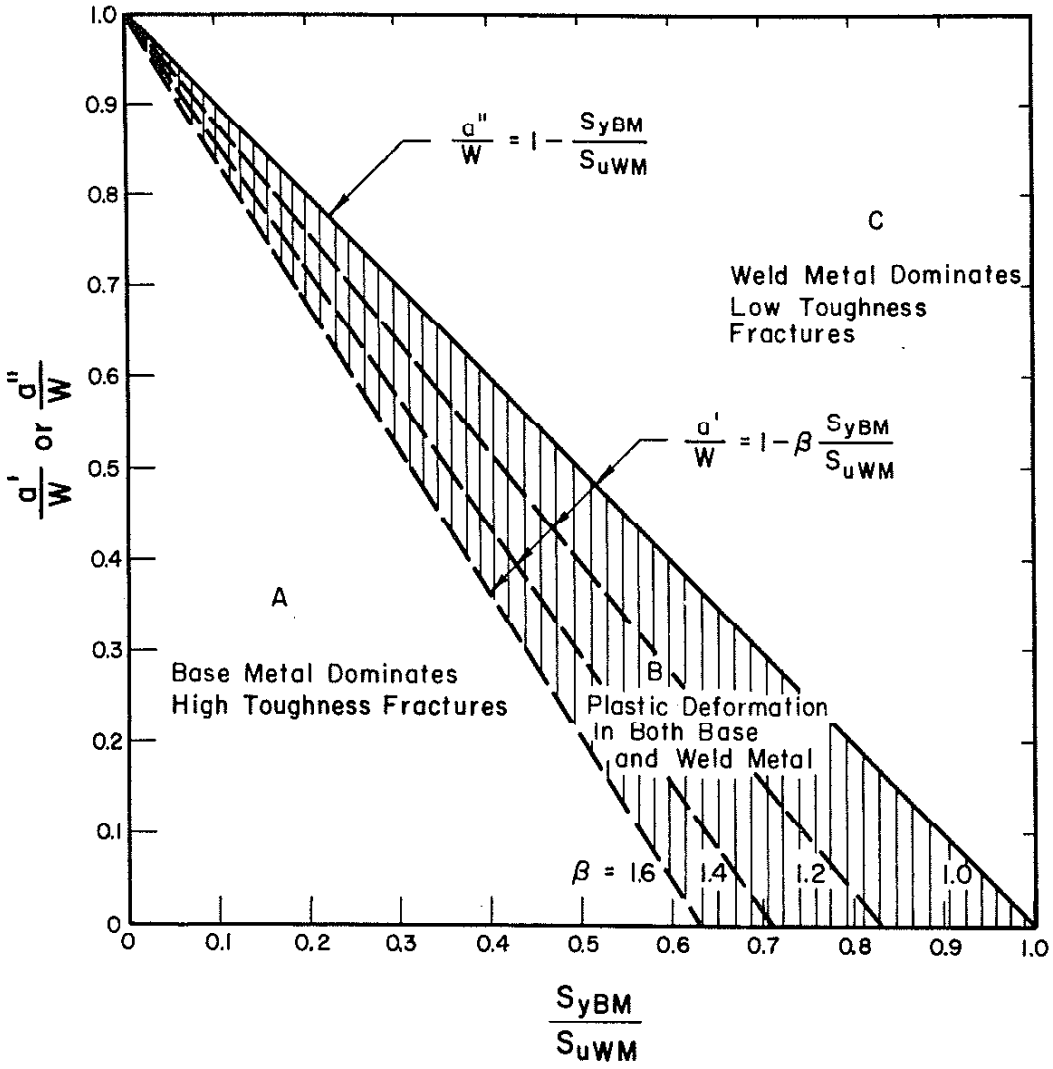

Fig. 19 The effects of weld metal overmatching and work hardening on the transition flaw widths a'/W and a"/W.

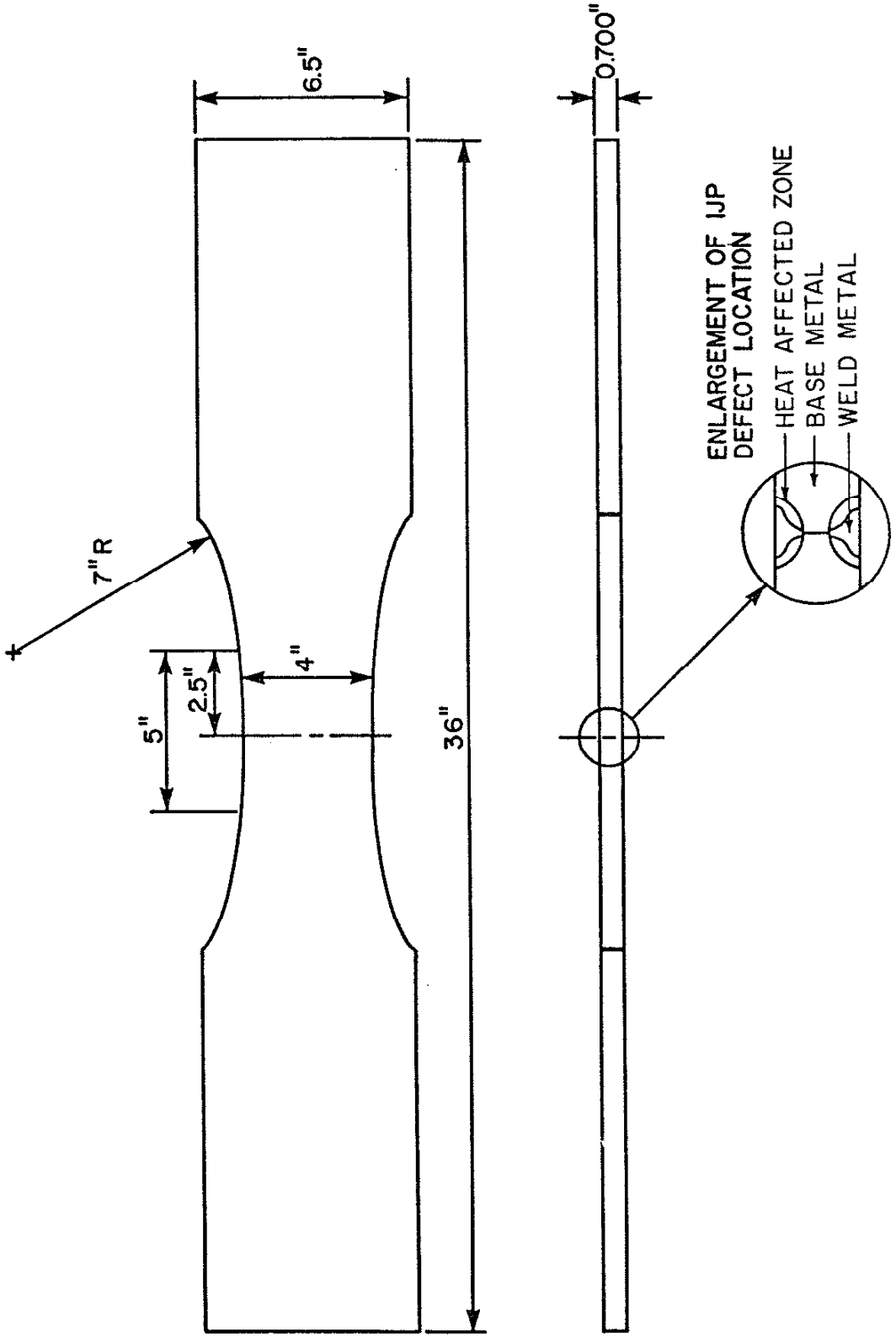

Fig. 20 Dimensions of butt welded A514F/E110 specimens containing incomplete joint penetration discontinuities.

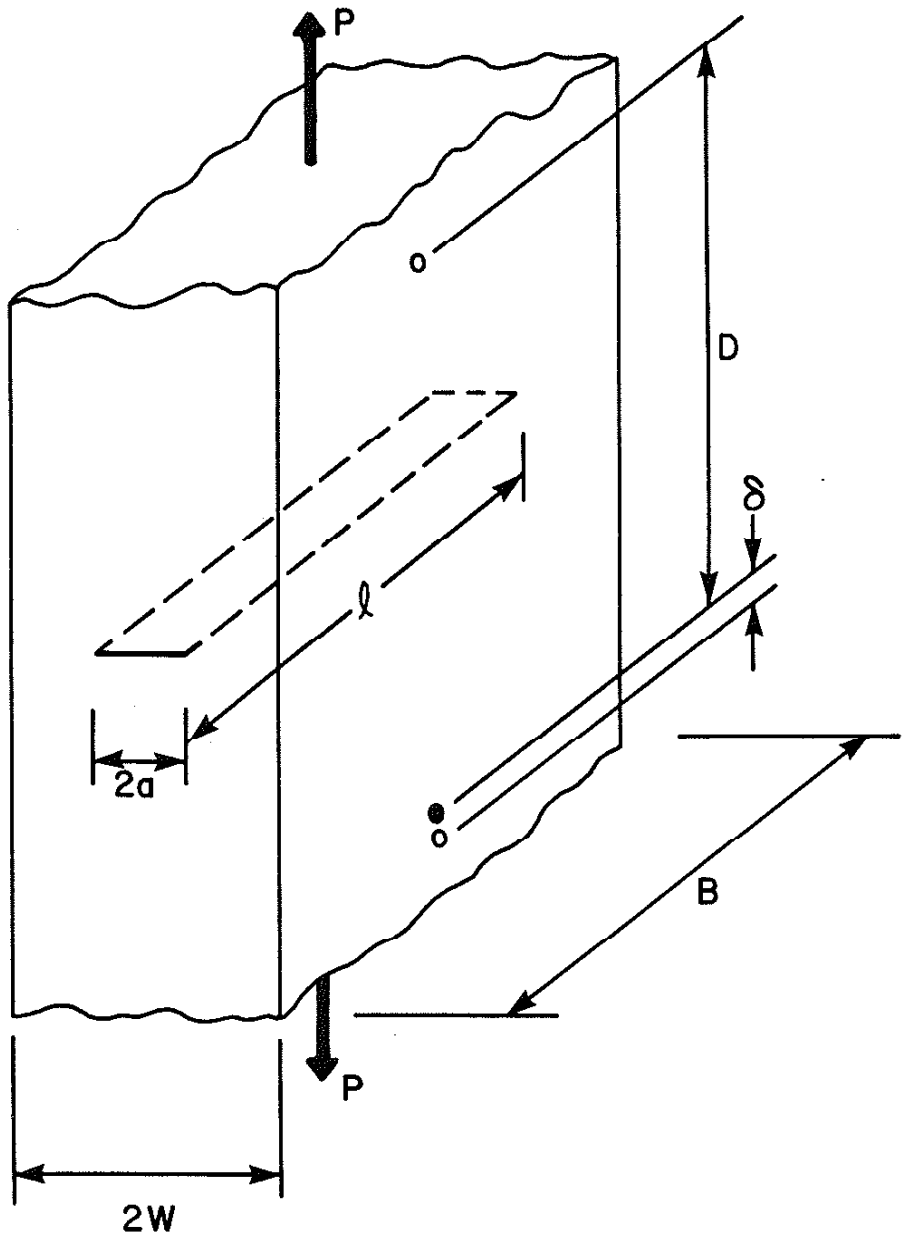

Fig. 21 Enlarged view of the test section shown in Fig. 20.

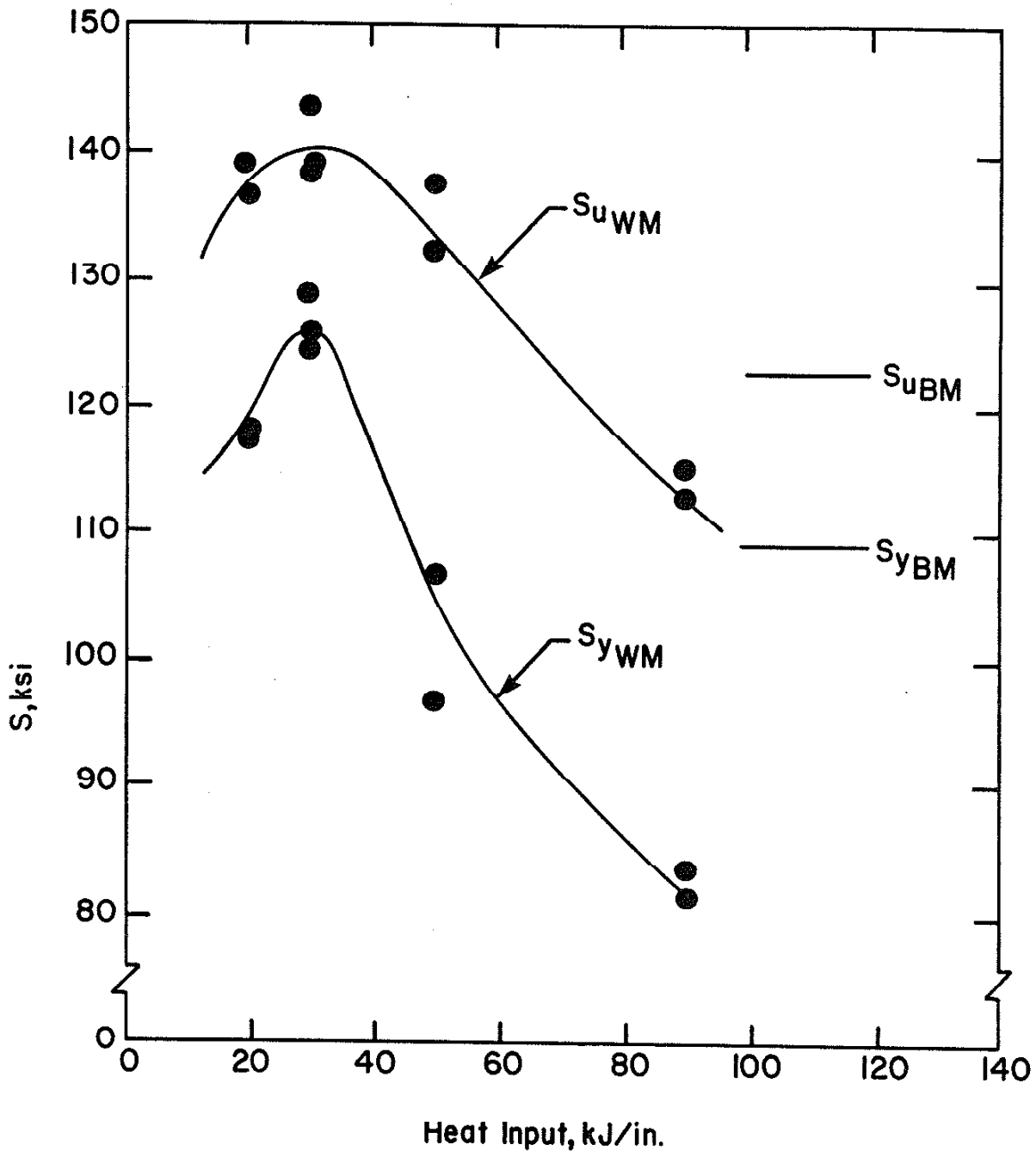

Fig. 22 The effect of welding heat input on the yield and tensile strengths of E110 weld metal.

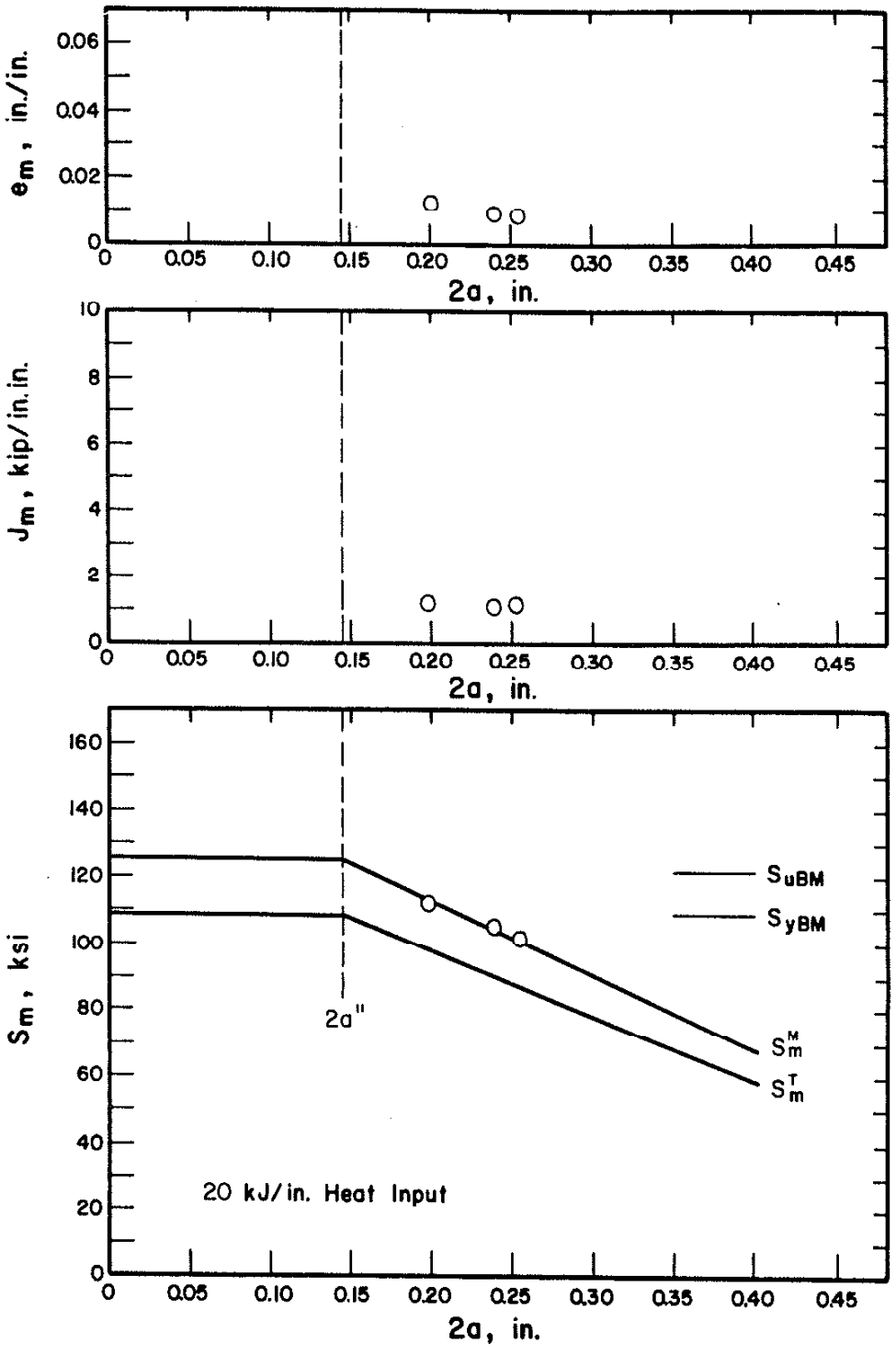

Fig. 23 Experimental results of specimens fabricated with 20 kJ/in. heat input welds. The collapse stress, S_m, data lie within the Tresca (S_m^T) and von Mises (S_m^M) limit load predictions.

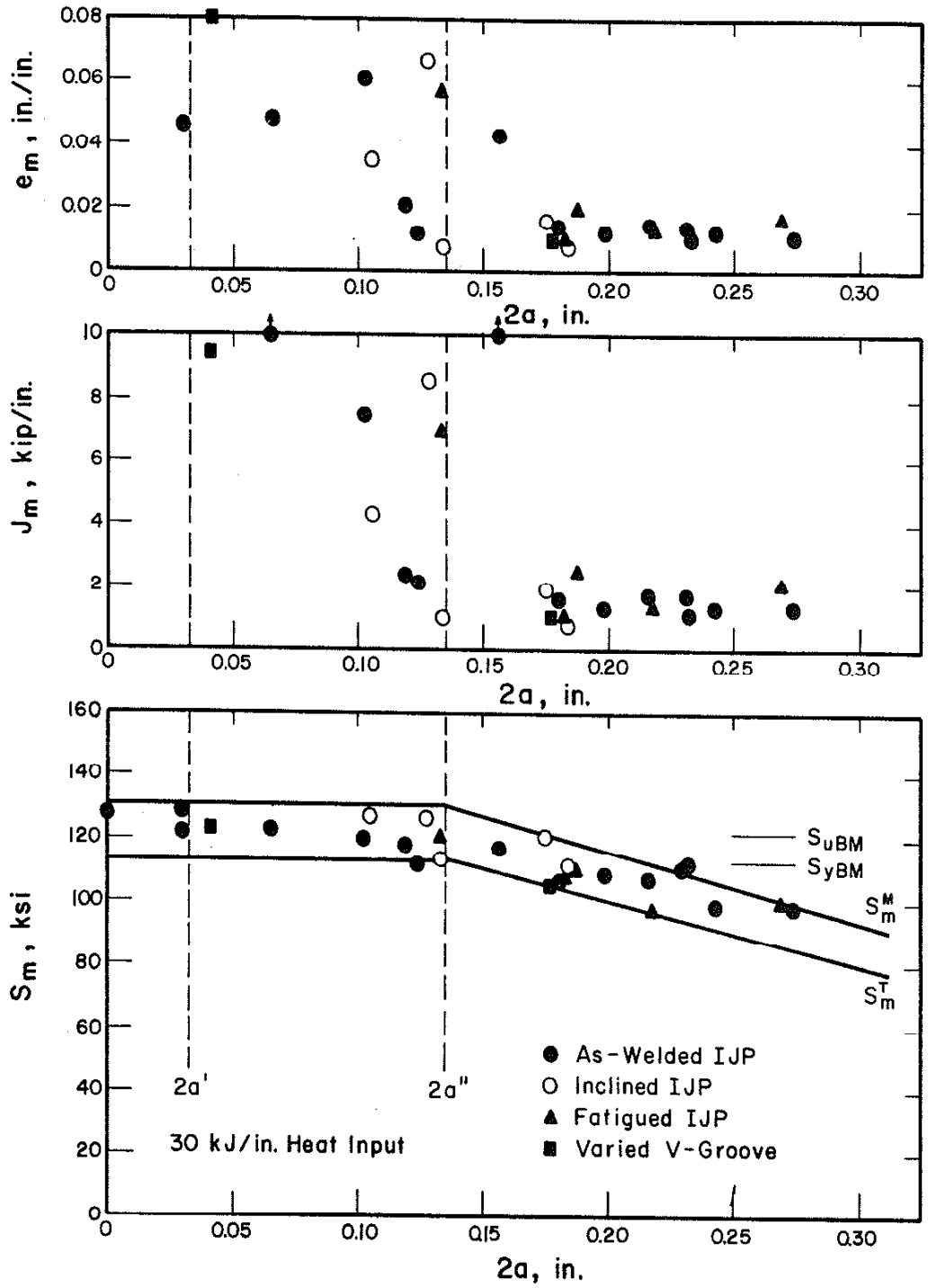

Fig. 24 Experimental results of specimens fabricated with 30 kJ/in. heat input welds. The collapse stress, S_m, data lie within the Tresca (S_m^T) and von Mises (S_m^M) limit load predictions. The strain at maximum load (e_m) and J-integral data show a transition from high to low values at the predicted flaw width, 2a".

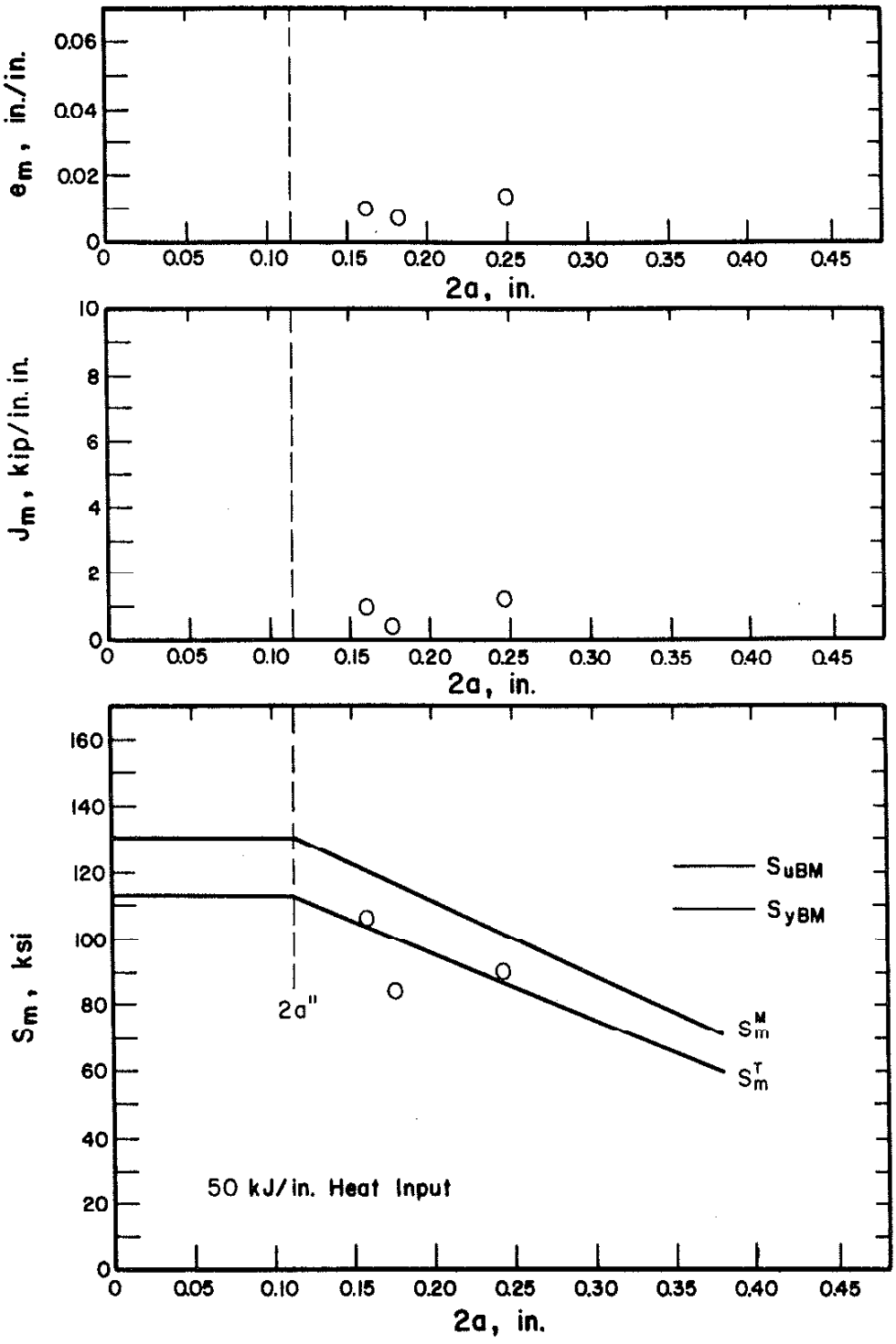

Fig. 25 Experimental results of specimens fabricated with 50 kJ/in. heat input welds. The low e_m, J_m and S_m data points resulted from a specimen containing a secondary flaw.

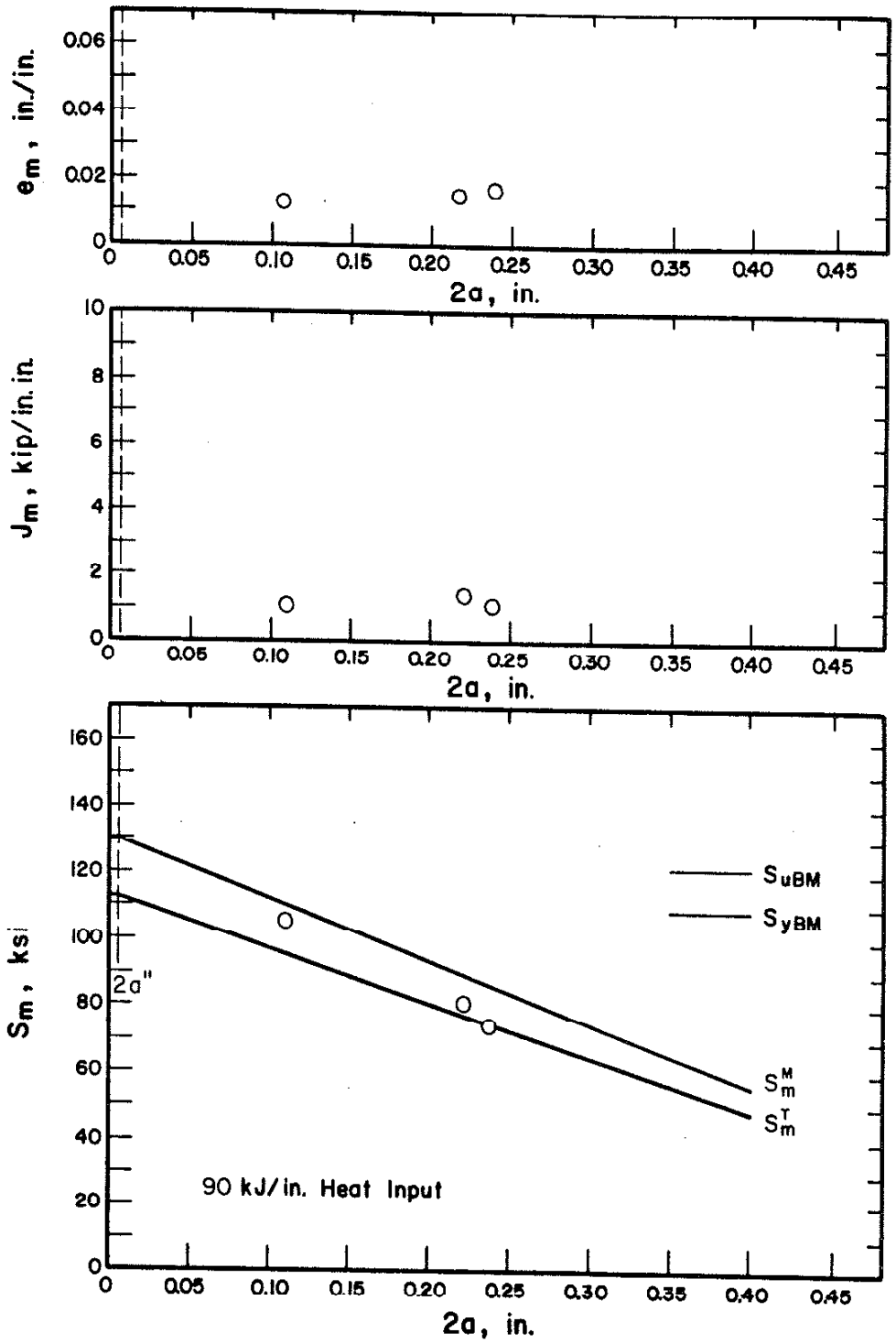

Fig. 26 Experimental results of specimens fabricated with 90 kJ/in. heat input welds. Note that the limit load failure criterion controls the fracture behavior over almost the entire range of 2a.

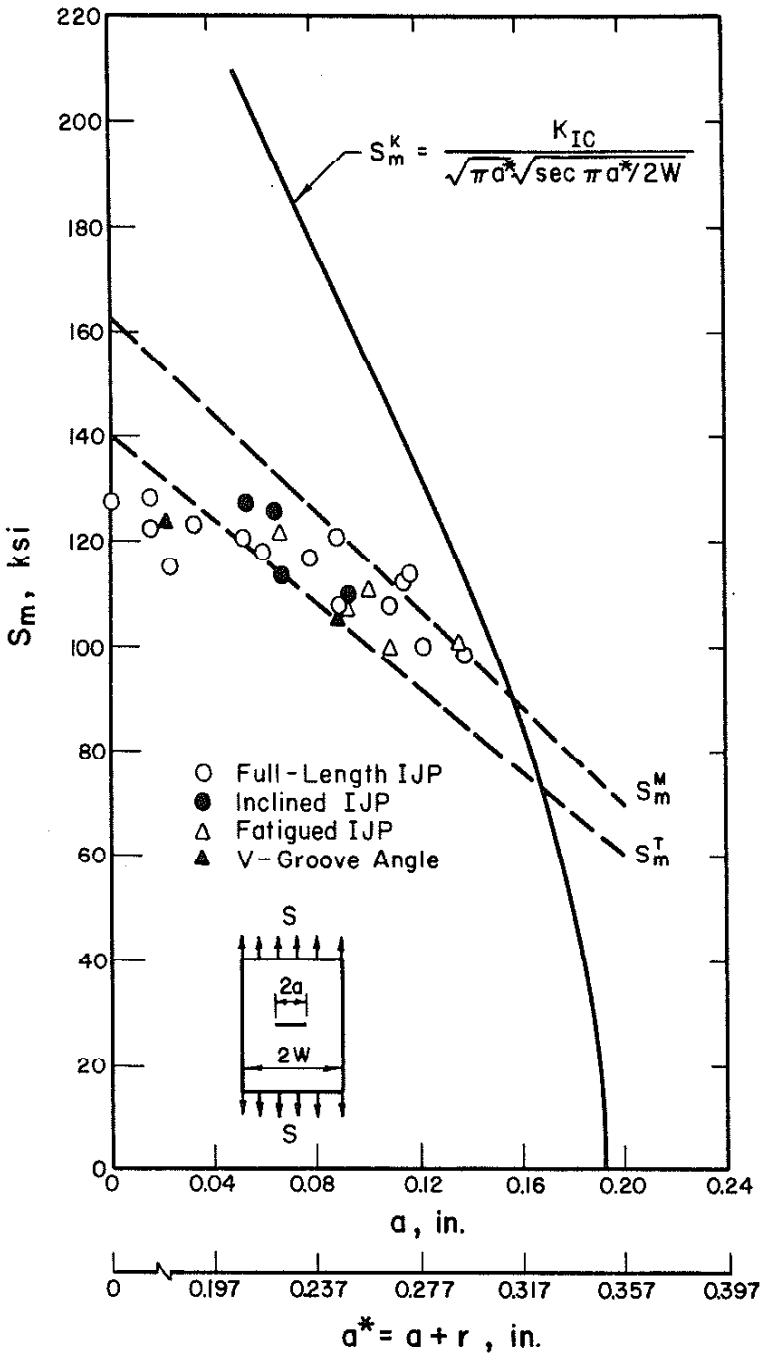

Fig. 27 Comparison of A514F/E110 flawed weldment data with collapse stresses predicted by the limit load and fracture toughness failure criteria. The S_m^K curve was corrected for the crack tip plastic zone.

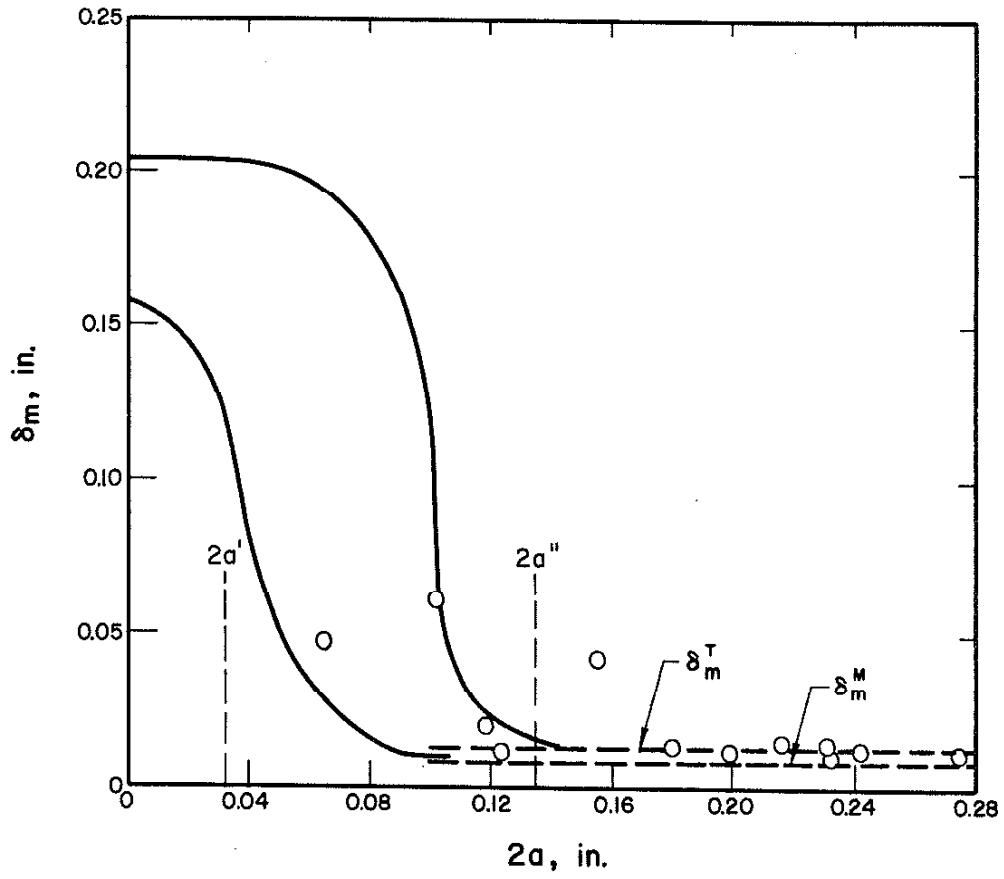

Fig. 28 Comparison of the deformation at collapse (δ_m) data with the values predicted for as-welded, 30 kJ/in. heat input weldments.

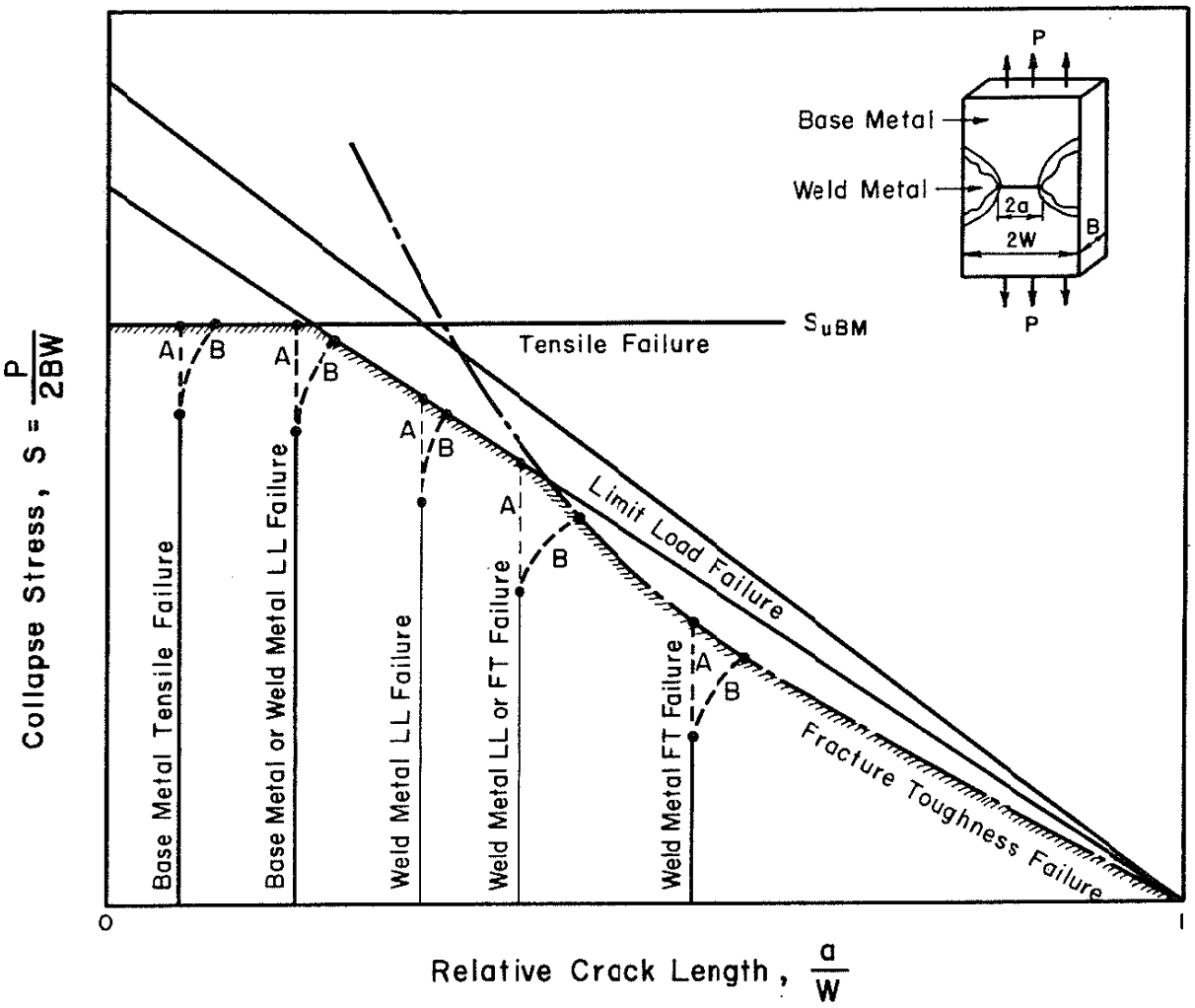

Fig. 29 The effects of subcritical crack extension on the two failure criteria model for a centrally flawed butt weldment. For a given initial crack length, specimens not undergoing subcritical crack extension follow trajectory A; while those that exhibit subcritical crack extension will follow a trajectory such as B.

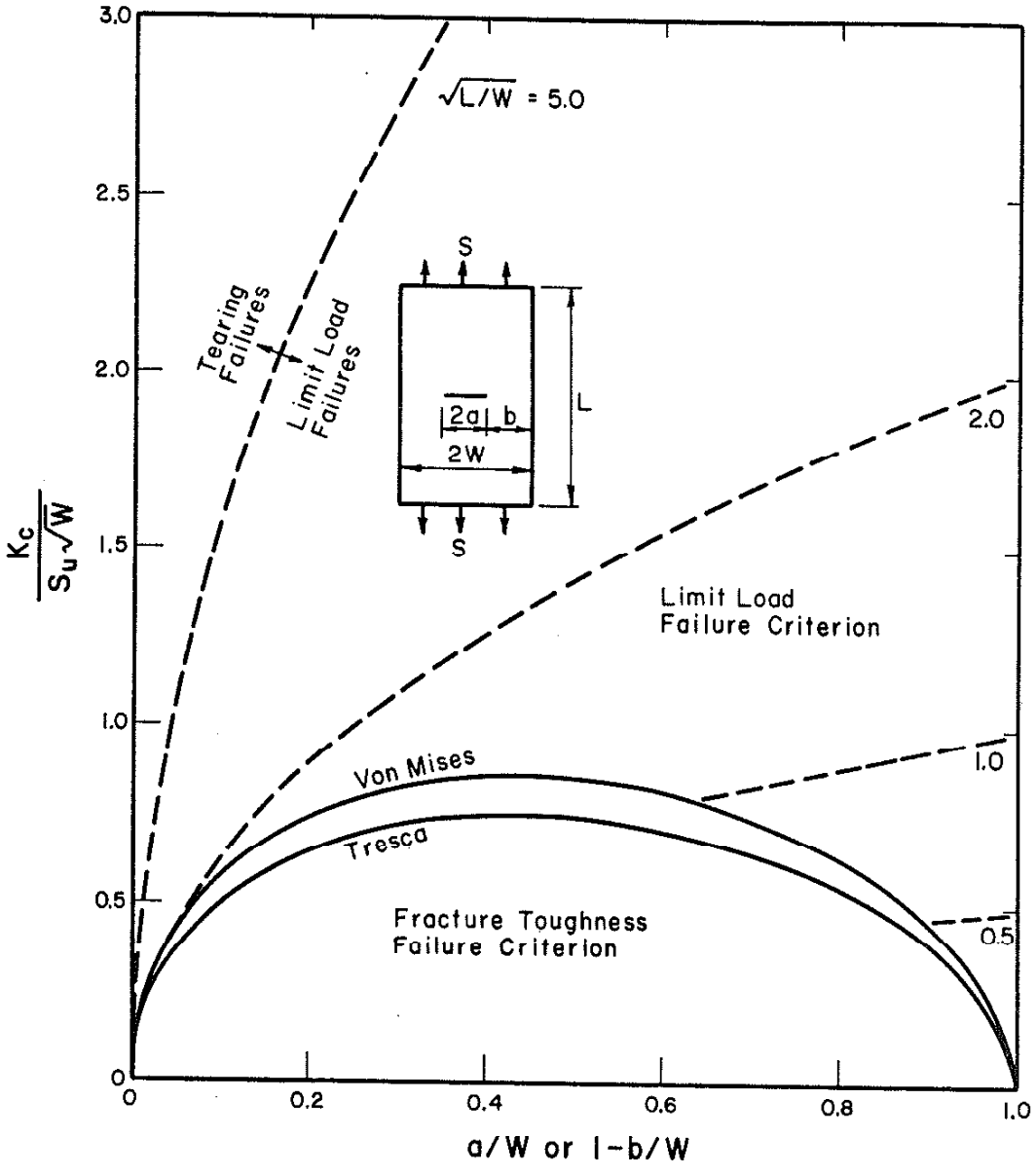

Fig. 30 The effects of stable tearing on the fracture behavior of center-crack tension specimens. Subcritical crack extension may occur at a constant value of $K_c/S_u\sqrt{W}$ until either the limit load or fracture toughness failure criterion controlled region is encountered.

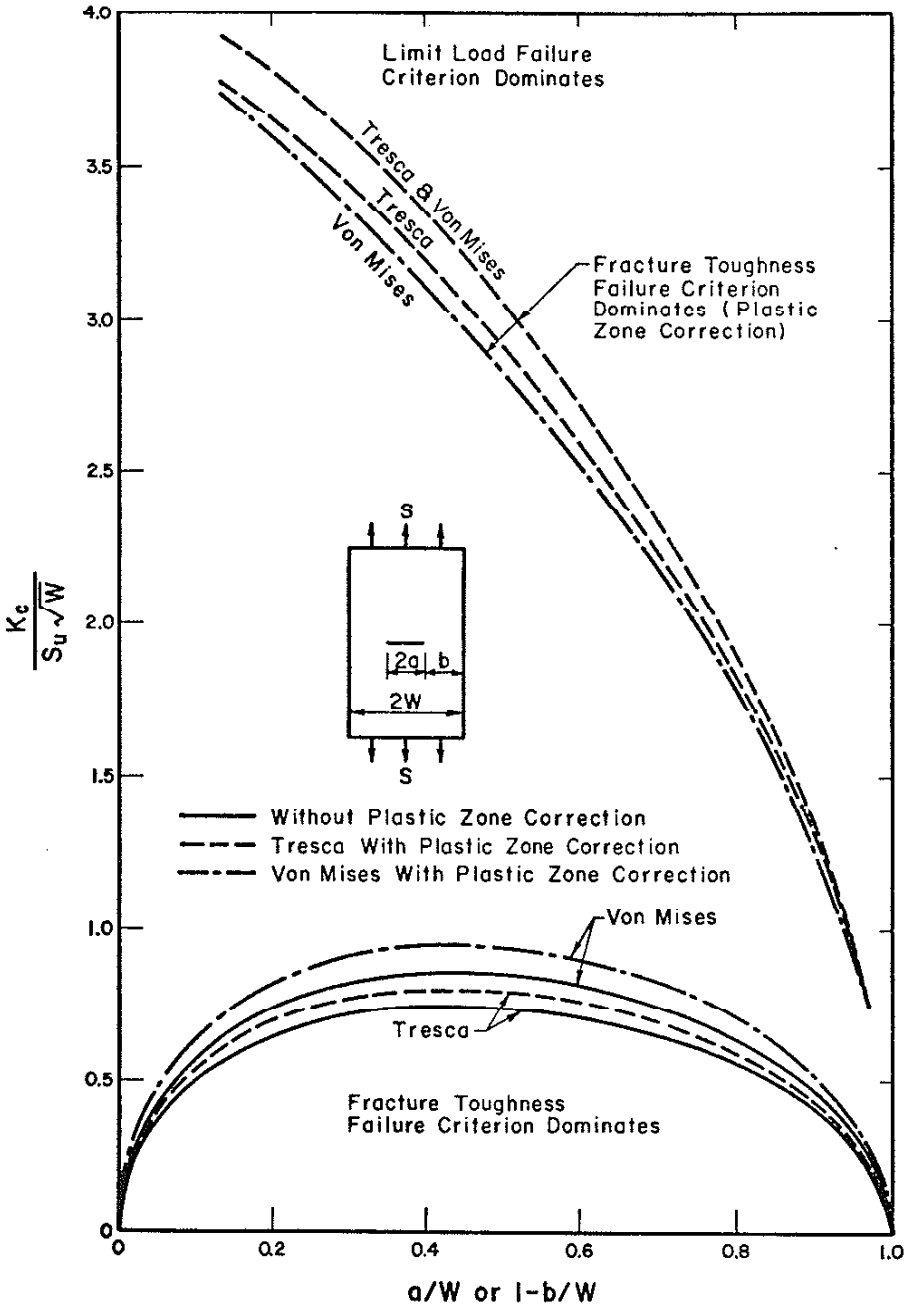

Fig. 31 The effects of crack tip plastic zone correction on the two failure criterion controlled regions for the center crack tension specimen. The acicular fracture toughness failure criterion region at large $K_c/S_u\sqrt{W}$ is believed to be an artifact of the plastic zone correction.

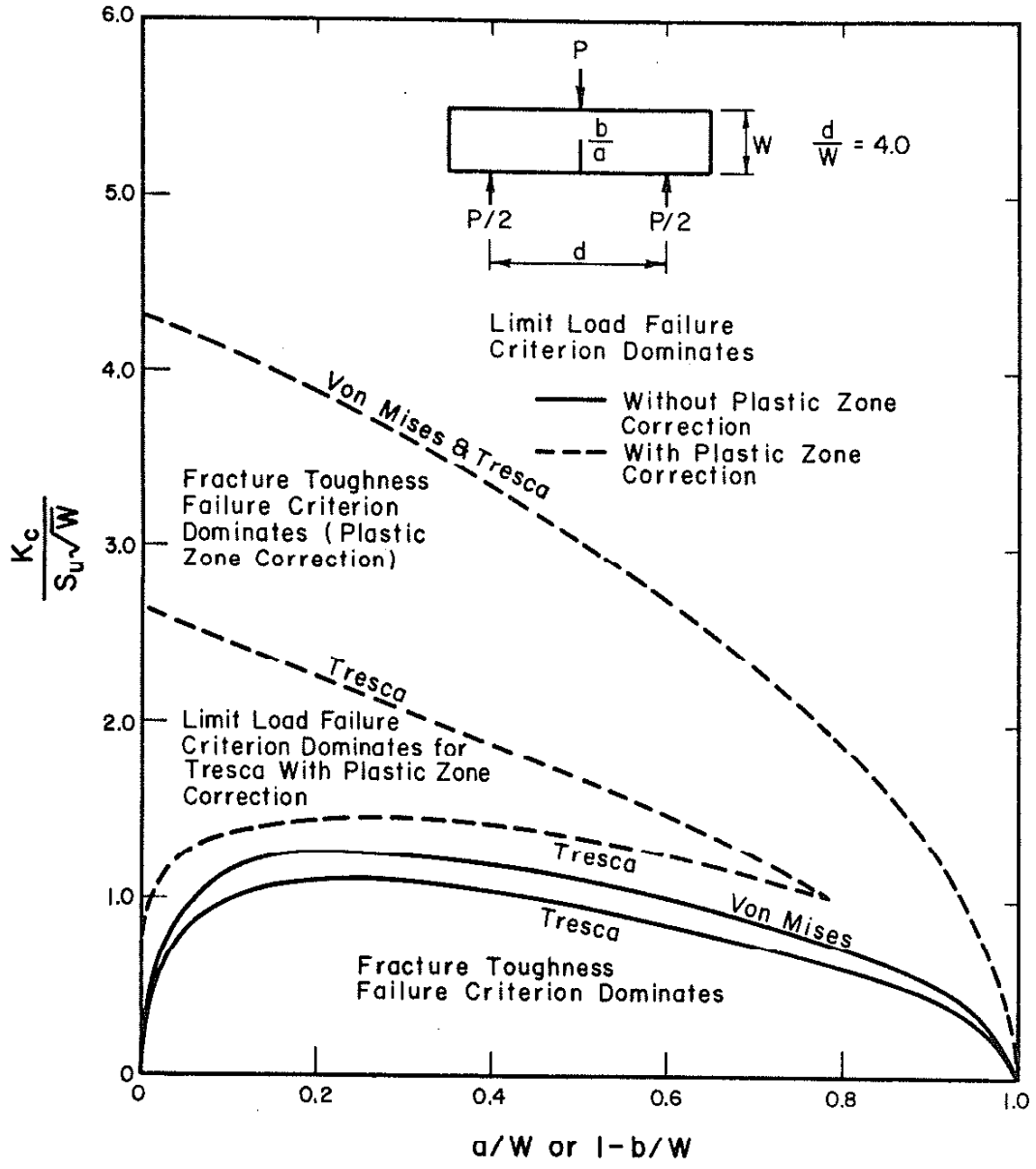

Fig. 32 The effects of crack tip plastic zone correction on the regions controlled by the two failure criteria for the three-point bend specimen. The regions within the dashed curves are believed to be artifacts of the plastic zone correction.

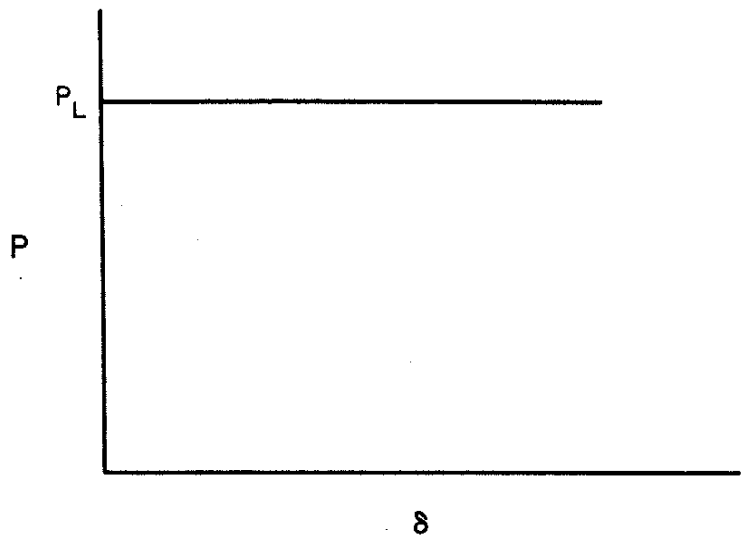

Fig. B1 Load versus deflection for a rigid-plastic material.

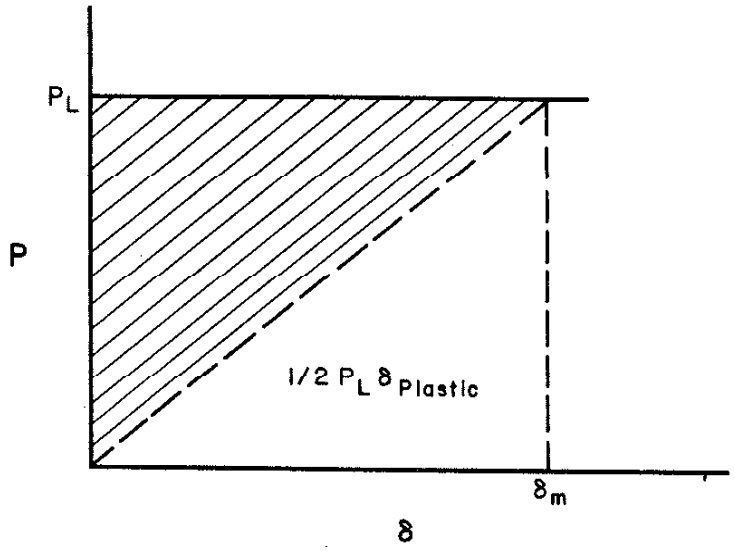

Fig. B2 Load versus deflection curve of a rigid-plastic material. The shaded area corresponds to the bracketed expression in Eq. B2.